CDF/DOC/BOTTOM/CDFR/9346
Version 5.0
March 2, 2009

Search for Exotic States in the $J/\psi\phi$ Mass Spectrum in Exclusive $B^+ \to J/\psi\phi K^+$ Decays in $p\bar{p}$ Collisions at $\sqrt{s} = 1.96$ TeV

Kai Yi[1], Jane Nachtman[2], Kwangzoo Chung[3]
Fermilab and University of Iowa

Ray Culbertson[4], Ting Miao[5]
Fermilab

Abstract

We report a search for exotic states in the mass spectrum of $J/\psi\phi$ through exclusive $B^+ \to J/\psi\phi K^+$ decays. This analysis is based on a 2.7 fb^{-1} data sample produced in $p\bar{p}$ collisions at $\sqrt{s} = 1.96$ TeV in CDF II experiment. We see evidence for a narrow structure at the $J/\psi\phi$ threshold with a measurement of mass as $4143.0 \pm 2.9(\text{stat}) \pm 1.2(\text{syst})$ MeV/c^2 and width as $11.7^{+8.3}_{-5.0}(\text{stat}) \pm 3.7(\text{syst})$ MeV/c^2. We oberve 14 ± 5 decays and the significance is estimated to be about 4.3 σ.

[1]yik@fnal.gov
[2]nachtman@fnal.gov
[3]kchung@fnal.gov
[4]rlc@fnal.gov
[5]tmiao@fnal.gov

Contents

1 Introduction

1.1 Motivation

Recent observations of new states such as X(3872), Y(3940), X(4160), Y(4260), Y(4320), Y(4660), Z(4430)$^+$ particles and anomalously large rates for $\Upsilon(5S) \to \Upsilon(1S, 2S)\pi^+\pi^-$ [1, 2, 3, 4, 5, 6, 7, 8] renewed the interests in quarkonium physics and exotic states. The interpretations of these new charmonium-like states vary among conventional charmonium [9], charmed hybrid [10], molecule [11] and four-quark state [12]. If $Y(4260)$ is a hybrid state, a triplet of states $(0^{-+}, 1^{-+}, 2^{-+})$ is expected near it [13]. Among them, the state with 1^{-+} is an exotic state (not allowed for $q\bar{q}$ states) and thus is clearly distinguished from conventional charmonia. The mass of 1^{-+} state has been predicted via different models to be in a wide range between 3.9 and 5.3 GeV/c^2 [14, 15]. Searches for such states have been performed through $B \to J/\psi\phi K$ decays [16, 17] following suggestion in reference [18]. A search through an exclusive process can potentially obtain clean signal if it is successful, but it can be limited due to available phase space or production mechanisms. On the other hand, an inclusive search can potentially offer a wider reach but with more background. The large B meson production rate and other potential production mechanisms at Tevatron provide us opportunities for search through both exclusive B decays and inclusive production. A new state decaying into $J/\psi\phi$ is also open to other exotic interpretations such as glueball, molecule, four-quark state, nuclear-bound quarkonium state predictions [19], as well as possibilities Beyond Standard Model (BSM) such as $S-$wave sbottomonium [20] and singlet scalar particle a_0 [21].

The CDF detector has excellent spatial (L_{xy}) resolution and excellent lepton particle identification. Furthermore, the COT and TOF sub-detectors also provide excellent Particle IDentification (PID) for protons and kaons. The selection of proton/kaon from dominant pion background can greatly reduce combinatorial background for the final states with proton/kaon particle(s). The studies of Λ_b [22] shows that we can reduce background by a factor of 4 and keep 60% of signal by identifying proton using combined TOF and dEdx information. In the cases of $J/\psi\phi$ and $J/\psi\phi K$ as final states, we can identify two or three kaons from the dominant pion background and expect great performance. We first search through exclusive B decays due to the large B meson production rates at Tevatron and its simplicity.

Besides $J/\psi\phi$ channel, other clean vector-vector meson final states at CDF also provide excellent opportunities for physics both in SM and BSM. For instance, there are predictions for nuclear-bound quarkonium states which decay into $J/\psi\phi$, $\phi\phi$ and $J/\psi J/\psi$ [19] and we can extend the vector mesons to $\Upsilon(nS)$. The anomalously large rate for $\Upsilon(5S) \to \Upsilon(1S, 2S)\pi^+\pi^-$ observed by Belle also stimulates us to search for $\Upsilon(nS)$ related channels. Since there is no precise prediction for the masses of $S-$wave sbottomonium and singlet scalar particle a_0, they open to all the above channels.

1.2 Dataset, Reconstruction Tool and Pre-selections

We use $\sim$2.7 fb^{-1} J/ψ sample (Di-muon trigger, p1-16) for this analysis. The BStntuple (6.14, v80) is used to reconstruct our channels. The tracks in each event are refitted to account for the energy lost in the detector material as muon and kaon. Two opposite-charged muons are used to form a J/ψ candidate with their mass between 2.8 and 3.75 GeV/c^2. The χ^2 of the J/ψ vertex fit is required to be less than 30. We then reconstruct $B^+ \to J/\psi K^+$, $B_s \to J/\psi\phi$ as our control samples and $B^+ \to J/\psi\phi K^+$ as our search channel.

To reconstruct a $B^+ \to J/\psi K^+$, we combine a J/ψ candidate with a charged track to a common vertex without applying PID but constraining the J/ψ mass to its PDG value in the fit. The maximum difference of Z_0 between tracks are required to be less than 1.5 cm, and the χ^2 of the fit is required to be less than 50. All $B^+ \to J/\psi K^+$ candidates with their mass between 5.0 and 5.6 GeV/c^2 are kept in the ntuple.

To reconstruct a $B_s \to J/\psi\phi$ candidate, we first reconstruct a J/ψ candidate as above and a $\phi \to K^+K^-$ candidate. The $\phi \to K^+K^-$ candidate is reconstructed by combining two opposite-charged kaon tracks (no PID) to form a common vertex. A ϕ candidates is defined by the following criteria: Z_0 between two tracks to be less than 1.5 cm, the χ^2 of the vertex fit to be less than 30 and the invariant mass of K^+K^- to be in the range between 0.98 and 1.06 GeV/c^2. A $B_s \to J/\psi\phi$ candidate is reconstructed by combining a J/ψ candidate and a ϕ candidate to a common vertex with J/ψ mass constrained to its PDG value. The maximum difference of Z_0 between tracks are required to be less than 1.5 cm and the χ^2 returned from the $J/\psi\phi$ vertex fit is required to be less than 50.

To reconstruct a $B^+ \to J/\psi\phi K^+$ candidate, we combine a reconstructed J/ψ candidate with its mass constrained to its PDG value, a reconstructed ϕ candidate and a charged kaon track (no PID) to form a common vertex. The J/ψ mass is reduced to be in the range between 2.9 and 3.3 GeV/c^2 before mass constraint and the ϕ mass is reduced to be in the range between 1.0 and 1.04 GeV/c^2 in order to reduce the disk space. The χ^2 returned from the fit to $J/\psi\phi K^+$ vertex is required to be less than 50 and the mass of $J/\psi\phi K^+$ is required to be between 5.0 and 5.6 GeV/c^2.

2 Study of Control Signals

The two key cuts in this analysis are the minimum L_{xy} of $B^+ \to J/\psi\phi K^+$ vertex and the minimum kaon PID LR (Likelihood Ratio, see CDF note 7488). By assuming 90% pions and 10% of protons for the non-Kaon background, the LR for each kaon is calculated based on TOF or dEdx only if the track has TOF or dEdx information only, otherwise it is calculated based on the combined TOF and dEdx information. We use $B_s \to J/\psi\phi$ and $B^+ \to J/\psi K^+$ channels as our control channels to study the performance of the two variables.

2.1 Control Signal I–$B_s \to J/\psi\phi$

2.1.1 Basic requirements

In order to study the performance of L_{xy} and kaon LR, we have the following basic requirements for a B_s candidate: The four tracks in the final state are required to have at least 4 silicon hits in the $r - \phi$ plane. The muon tracks are required to have at least 20 COT axial hits and the kaon tracks are required to have a minimum p_T of 250 MeV/c^2. The fit probability of J/ψ or ϕ vertex is required to be greater than 0.1% and the fit probability of $J/\psi\phi$ vertex is required to be greater than 1%. The p_T of the $J/\psi\phi$ object is required to be greater than 4 GeV/c^2. We define J/ψ (before mass constraint) and ϕ mass window as within 50 MeV/c^2 and 7 MeV/c^2 of their nominal (PDG) values.

2.1.2 Extract B_s parameters from Data

In order to extract the mass and width of B_s, we further require the L_{xy} of $J/\psi\phi$ vertex to be greater than 500 μm. We do a unbinned log-likelihood fit to the mass distribution of $J/\psi\phi$ as shown in Fig. 1 using RooFit. The B_s signal Probability Density Function (PDF) is a Gaussian function and the background PDF is a first-order Chebychev polynomial function. The mass and width returned from the fit are 5.366 ± 0.000 GeV/c^2 and 8.9 ± 0.3 MeV. We fix the mass and width of B_s to the above values in later fits.

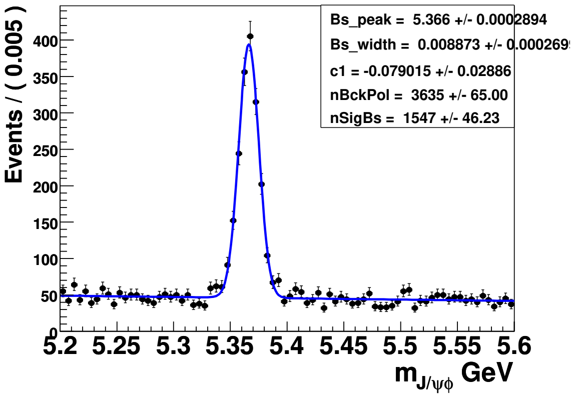

Figure 1: The $J/\psi\phi$ mass after the basic requirements and $L_{xy} > 500$ μm requirement.

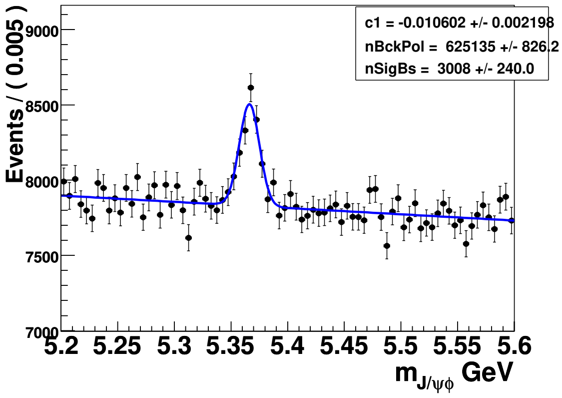

Figure 2: The $J/\psi\phi$ mass after the basic requirements. The reference point 1.

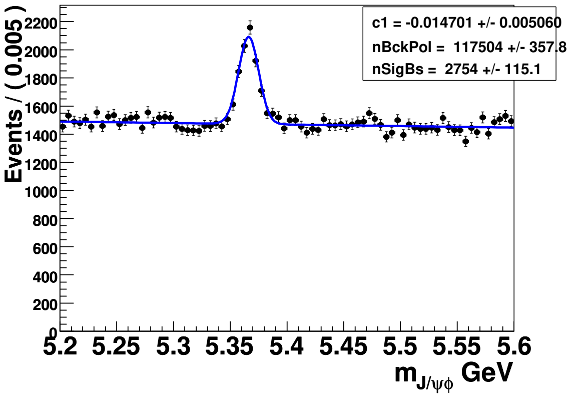

Figure 3: The $J/\psi\phi$ mass after the basic requirements and $L_{xy} > 50$ μm requirement. The reference point 2.

2.1.3 The number of B_s signals at reference points

We use the number of B_s signal with basic requirements as the reference point (point 1) for L_{xy} performance studies and the number of B_s signal with basic requirements and $L_{xy} > 50$ μm requirement as the reference point (point 2) for kaon PID LR performance studies. The fits to the $J/\psi\phi$ masses of the two reference points are shown in Fig. 2 and 3. We have 3008 ± 240 events at point 1 and 2754 ± 115 events at point 2.

2.1.4 Efficiency vs L_{xy} and Kaon PID LR

The B_s select efficiency as a function of its minimum L_{xy} and minimum kaon LR (apply to both kaons) are shown in Fig. 4 and 5. We have about 90% select efficiency for a minimum L_{xy} of 100 μm and above 60% select efficiency for a minimum kaon LR of 0.0 for both kaon tracks. We also examined the select efficiencies for kaon LR in the first (p1-10) and second half (p11-16) of the dataset which are shown in Fig. 6 and 7. They are pretty close in the region of interest (around zere [6]). It is slightly better in the second half of the data.

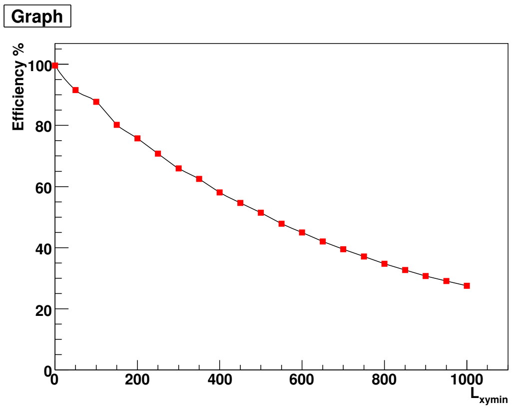

Figure 4: The B_s efficiency as a function of its minimum L_{xy} w.r.t point 1.

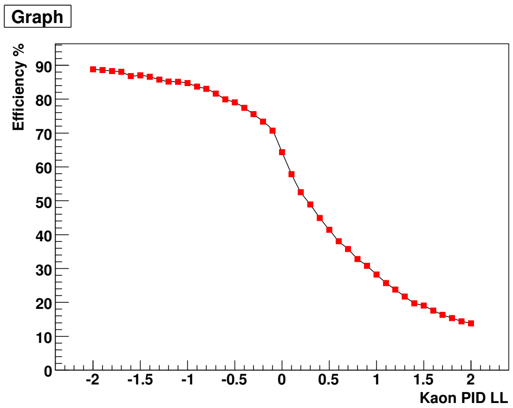

Figure 5: The B_s efficiency as a function of minimum kaon LR w.r.t point 2.

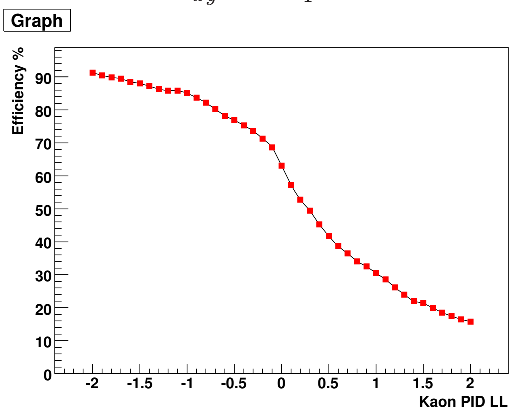

Figure 6: The B_s efficiency as a function of minimum kaon LR w.r.t point 2 in the first half of the dataset.

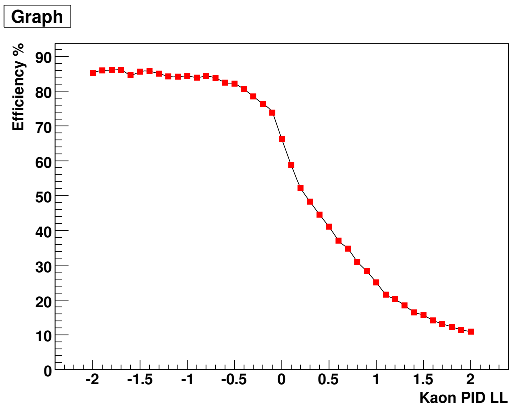

Figure 7: The B_s efficiency as a function of minimum kaon PID LR w.r.t point 2 in the second half of the dataset.

[6]The kaon logged LR need to be greater than zero for a track to be more likely to be a kaon.

As a comparison, we show the invariant masses of $J/\psi\phi$ in Fig. 8, 9, 10 and 11 at reference points and the following two choices: minimum L_{xy} of 100 μm and minimum kaon LR of zero. The cut of $L_{xy} > 100$ μm keeps about 88% of the B_s signal while reduces the background level by a factor of 13. The minimum kaon LR of zero keeps about 64% of the B_s signal while reduces the background level by a factor of 30.

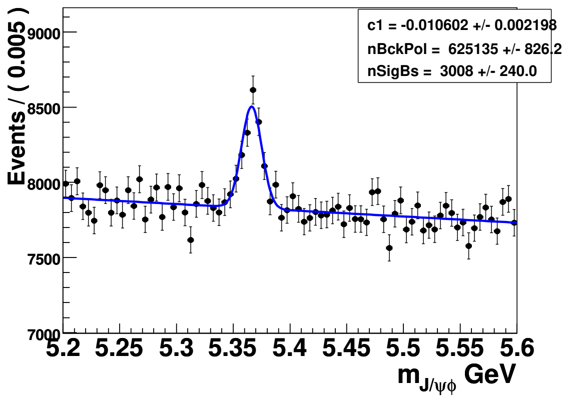

Figure 8: The $J/\psi\phi$ mass after the basic requirements. The reference point for L_{xy}.

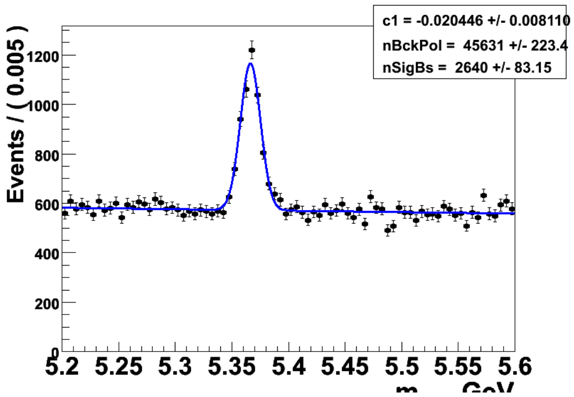

Figure 9: The $J/\psi\phi$ mass after the basic and $L_{xy} > 100$ μm requirements.

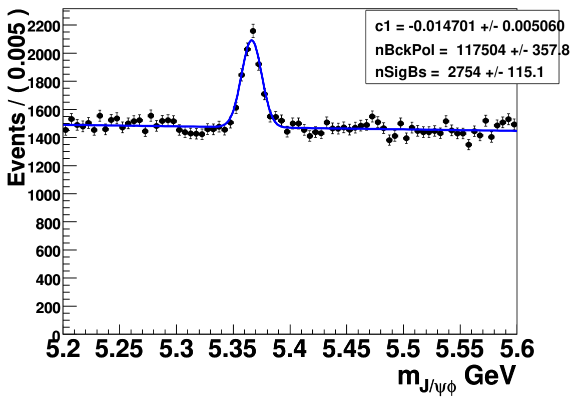

Figure 10: The $J/\psi\phi$ mass after the basic and $L_{xy} > 50$ μm requirements. The reference point for kaon PID LR.

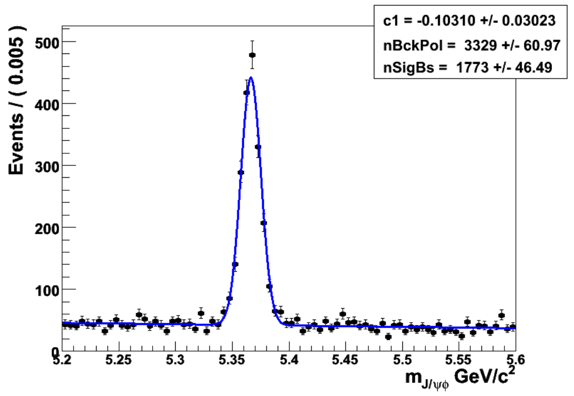

Figure 11: The $J/\psi\phi$ mass after the basic and kaon LR > 0.0 requirements.

2.2 Control Signal II–$B^+ \to J/\psi K^+$

2.2.1 Basic requirements

The basic requirements for a $B^+ \to J/\psi K^+$ candidate are: The three tracks in the final state are required to have at least 4 silicon hits in the $r-\phi$ plane. The muon tracks are required to have at least 20 COT axial hits and the kaon track is required to have a minimum p_T of 250 MeV/c^2. The fit probability of J/ψ vertex is required to be greater than 0.1% and the fit probability of $J/\psi K^+$ vertex is required to be greater than 1%. The p_T of the $J/\psi K^+$ object is required to be greater than 4 GeV/c^2. We define J/ψ (before mass constraint) as within 50 MeV/c^2 of its nominal (PDG) value.

2.2.2 Extract B^+ parameters from Data

We use the same way to extract the B^+ parameters from data as we did in the B_s channel: do a free fit to the $J/\psi K^+$ mass distribution by requiring its L_{xy} to be greater than 500 μm. Fig. 12 shows the fit and the returned parameters. The B^+ signal PDF is a Gaussian function and the background PDF is a first-order Chebychev polynomial function. The mass and width returned from the fit are 5.278 ± 0.000 GeV/c^2 and 11.5 ± 0.1 MeV. We fix the mass and width of B^+ to the above values in later fits.

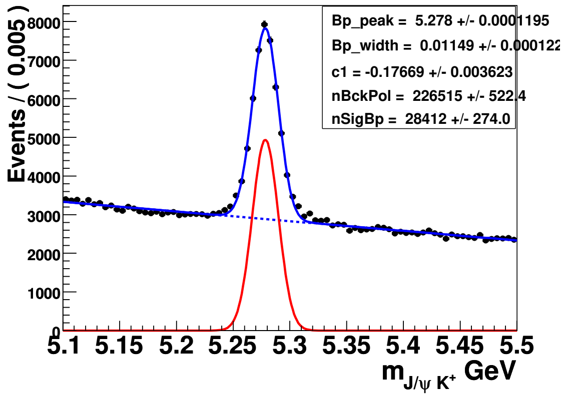

Figure 12: The $J/\psi K^+$ mass after the basic and $L_{xy} > 500$ μm requirements.

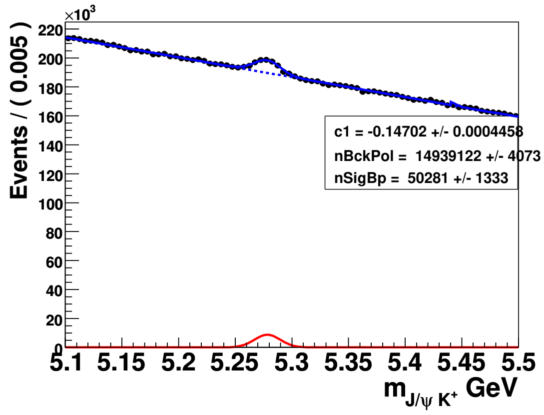

Figure 13: The $J/\psi K^+$ mass after the basic requirements. The reference point for L_{xy}.

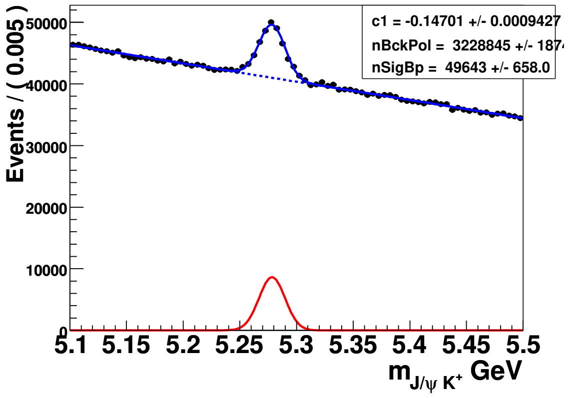

Figure 14: The $J/\psi K^+$ mass after the basic and $L_{xy} > 50$ μm requirements. The reference point for kaon LR.

2.2.3 The number of B^+ signals at reference points

We use the number of B^+ signal with basic requirements as the reference point (point 1) for L_{xy} performance studies and the number of B^+ signal with basic requirements and $L_{xy} > 50$ μm requirement as the reference point (point 2) for kaon LR performance studies. The fits to the $J/\psi K^+$ masses of the two reference points are shown in Fig. 13 and 14. We have 50281 ± 1333 events at point 1 and 49643 ± 658 events at point 2.

2.2.4 Efficiency vs L_{xy} and Kaon PID LR

The B^+ select efficiency as a function of its minimum L_{xy} and minimum kaon LR are shown in Fig. 15 and 16. And we have about 90% select efficiency for a minimum L_{xy} of 100 μm and above 80% select efficiency for a minimum kaon PID LR of 0.0 for the kaon track. We also examined the select efficiencies for kaon LR in the first (p1-10) and second (p11-16) half of the dataset which are shown in Fig. 17 and 18. They are pretty close in the region of interest (around zero). It is slightly better in the first half of the data.

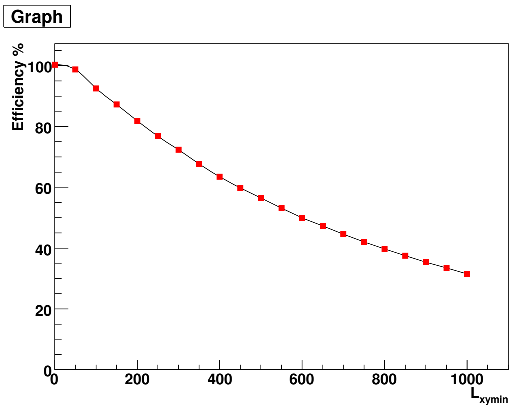

Figure 15: The B^+ efficiency as a function of its minimum L_{xy} w.r.t point 1.

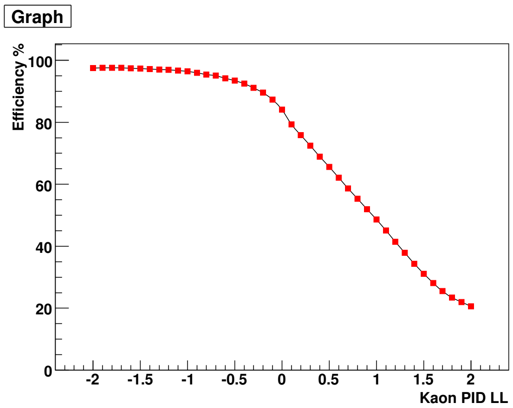

Figure 16: The B^+ efficiency as a function of minimum kaon LR w.r.t point 2.

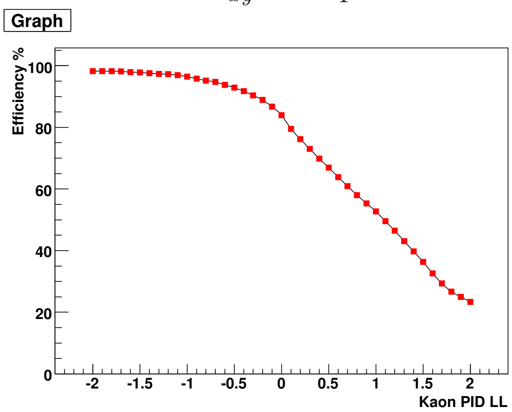

Figure 17: The B^+ efficiency as a function of minimum kaon LR w.r.t point 2 in the first half of the dataset.

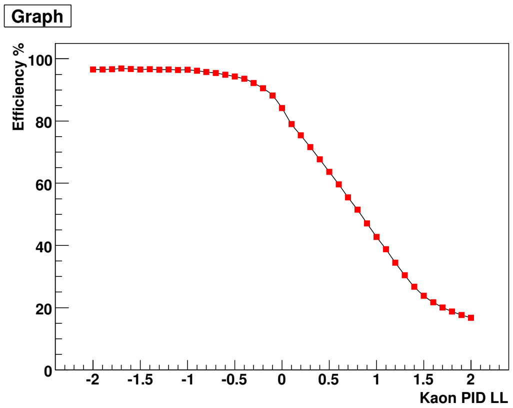

Figure 18: The B^+ efficiency as a function of minimum kaon LR w.r.t point 2 in the second half of the dataset.

As a comparison, we show the invariant masses of $J/\psi K^+$ in Fig. 19, 20, 21 and 22 at reference points and the following two choices: minimum L_{xy} of 100 μm and minimum kaon PID LR of zero. The cut of $L_{xy} > 100$ μm keeps about 93% of the B^+ signal while reduces the background level by a factor of 11. The minimum kaon LR of zero keeps about 84% of the B^+ signal while reduces the background level by a factor of 6.

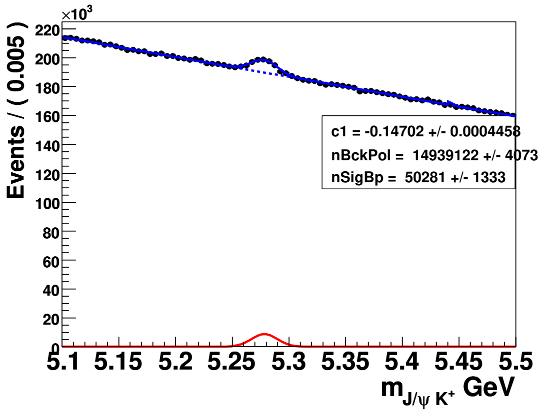

Figure 19: The $J/\psi K^+$ mass after the basic requirements. The reference point for L_{xy}.

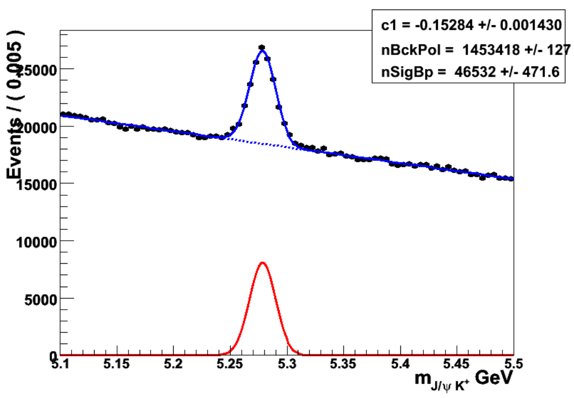

Figure 20: The $J/\psi K^+$ mass after the basic and $L_{xy} > 100$ μm requirements.

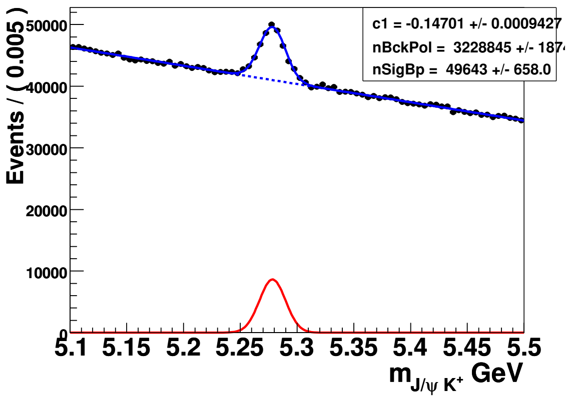

Figure 21: The $J/\psi K^+$ mass after the basic and $L_{xy} > 50$ μm requirements. The reference point for kaon LR.

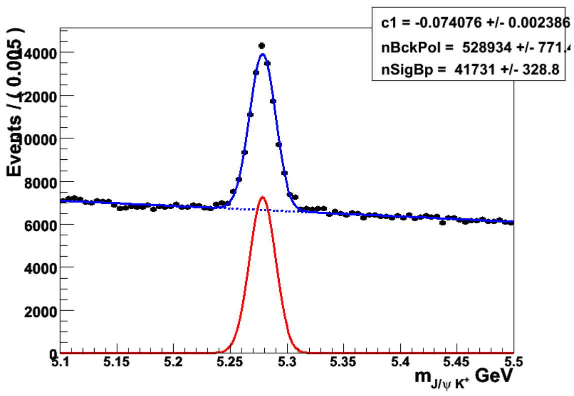

Figure 22: The $J/\psi K^+$ mass after the basic and kaon LR > 0.0 requirements.

2.3 Preliminary Investigation of $B^+ \to J/\psi\phi K^+$

We have excellent separation between $B^+ \to J/\psi\phi K^+$ and combinatorial background at CDF by combining minimum L_{xy} and kaon PID LR requirements. As a starting point, we choose the minimum L_{xy} as 100 μm and minimum kaon PID LR as 0.0 for our search channel $B^+ \to J/\psi\phi K^+$. Based on the performance studies on the control samples, we estimate (ignore momentum dependence) a signal select efficiency of about $0.93 \times 0.64 \times 0.84$=50% and a background reduction factor of about $11 \times 30 \times 6$=2000. This is already spectacular and there is even more potential at CDF for PID and spectroscopy. We see a new avenue for CDF physics.

The basic requirements for $B^+ \to J/\psi\phi K^+$ are: The five tracks in the final state are required to have at least 4 silicon hits in the $r - \phi$ plane. The muon tracks are required to have at least 20 COT axial hits and the kaon tracks are required to have a minimum p_T of 250 MeV/c^2. The fit probability of J/ψ or ϕ vertex is required to be greater than 0.1% and the fit probability of $J/\psi\phi K^+$ vertex is required to be greater than 1%. The p_T of the $J/\psi\phi K^+$ object is required to be greater than 4 GeV/c^2. We define J/ψ (before mass constraint) and ϕ mass window as within 50 MeV/c^2 and 7 MeV/c^2 of their nominal (PDG) values. The invariant mass of $J/\psi\phi K^+$ after basic requirements and after adding the above L_{xy} and kaon LR cuts are shown in Fig. 23 and 24. Although we can not have a estimation of signal efficiency due to the huge background, but the background reduction factor is close to our estimation–a factor of about 2000. We are going to use these cuts as the starting point for MC studies.

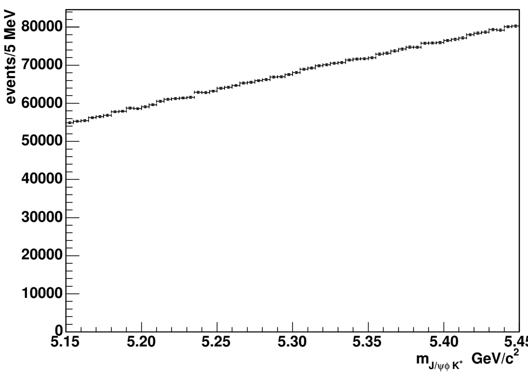

Figure 23: The $J/\psi\phi K^+$ mass after the basic requirements.

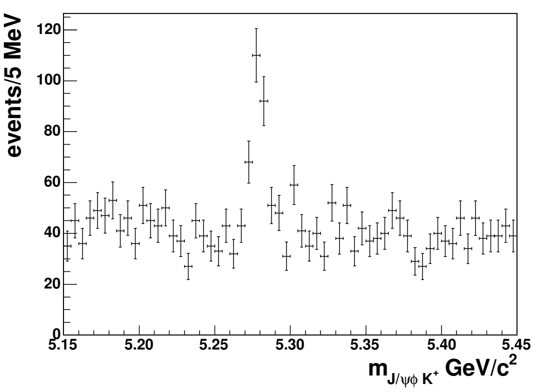

Figure 24: The $J/\psi\phi K^+$ mass after the basic cuts, $L_{xy} > 100$ μm and kaon LR ≥ 0.0 for three kaon tracks.

For the purpose of investigating the potential number of $B^+ \to J/\psi\phi K^+$ signals, we loose the minimum kaon LR to -1.0 and the minimum silicon hits in the $r-\phi$ plane for each track to 3. The invariant mass of $J/\psi\phi K^+$ with these loose cuts is shown in Fig. 25. An unbinned log-likelihood fit gives us a yield of 344 ± 42 events[7], that is to say, we have at least 344 potential $B^+ \to J/\psi\phi K^+$ signal available. This is the largest $B^+ \to J/\psi\phi K^+$ sample in the world, however, the background level is too high for structure search in the $J/\psi\phi$ mass spectrum, we need to adjust our cuts to suppress the background.

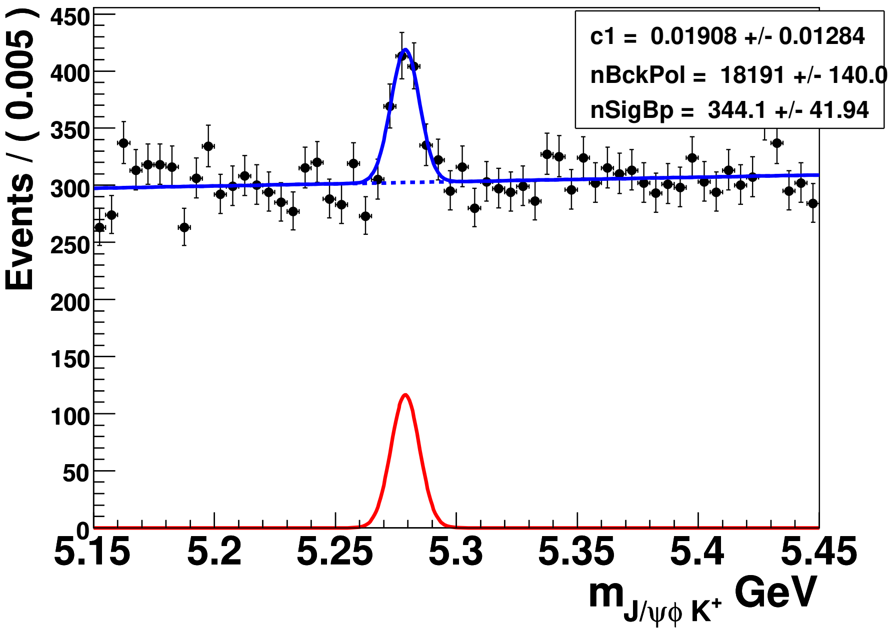

Figure 25: The $J/\psi\phi K^+$ mass with loose kaon LR and silicon requirements.

[7]The B^+ signal PDF is a Gaussian function with its mass fixed to PDG value and its width fixed to 5.9 MeV obtained from MC in next chapter, the background function is a first-order Chebychev polynomial function.

3 MC Studies and the Justification of Cuts

3.1 Studies of $B^+ \to J/\psi\phi K^+$ MC in the phase space

Following the CDF b-Group MonteCarlo page, we generated about half million $B^+ \to J/\psi\phi K^+$ MC events in the phase space using release 6.1.4mc. We use TPidSim package to simulate TOF and dEdx information.

3.1.1 Mass Resolution of $B^+ \to J/\psi\phi K^+$

The invariant mass of $J/\psi\phi K^+$ for MC events generated in phase space after applying the basic cuts, L_{xy} and kaon LR at the starting point is shown in Fig. 26. We do a unbinned log-likelihood fit to the mass distribution of $J/\psi\phi K^+$. The B^+ signal PDF is a Gaussian function with the mass fixed to its PDG value and the background PDF is a first-order Chebychev polynomial function. The returned width from the fit is 5.9 ± 0.0 MeV, we fix the B^+ width as 5.9 MeV in the fits to data later. The mass resolution for $B^+ \to J/\psi\phi K^+$ (5.9 MeV) is significantly better than $B^+ \to J/\psi K^+$ (11.5 MeV).

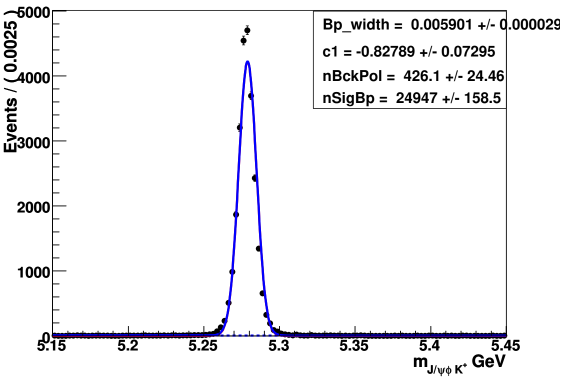

Figure 26: The $J/\psi\phi K^+$ mass in the MC sample generated in phase space after the basic cuts, L_{xy} and kaon LR cuts at the starting point.

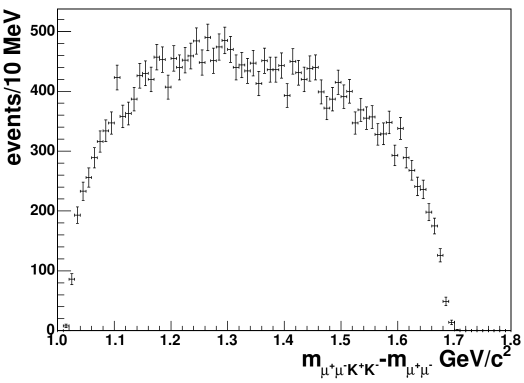

Figure 27: The mass difference between $J/\psi\phi$ and J/ψ in the B mass window after the basic cuts, L_{xy} and kaon LR cuts at the starting point (phase space MC).

3.1.2 First Check of Acceptance

We define the $B^+ \to J/\psi\phi K^+$ mass window as within 3 σ of its PDG value. In order to take a quick check of the possible artifacts due to CDF detector acceptance, we plot the invariant mass difference between $J/\psi\phi$ and J/ψ in the defined B mass window for the MC events generated in phase space after applying the basic cuts, L_{xy} and kaon LR cuts at the starting point as in Fig. 27. There is no structure shown in the distribution due to CDF detector acceptance.

3.2 Mass Resolution of Potential Structures decays into $J/\psi\phi$

The mass resolution of a structure Y ($Y \to J/\psi\phi$) varies with its mass depending on its closeness to $J/\psi\phi$ threshold. We generated MC of $B \to YK^+, Y \to J/\psi\phi$ assuming the following masses for Y: 4.15, 4.25, 4.35, 4.45, 4.55, 4.65, 4.75 GeV/c^2. The width of each Y mass assumption is set to be zero. The mass difference between $J/\psi\phi$ and J/ψ in the defined B mass window is shown in Fig. 28. We use a Gaussian function as Y signal PDF and a first-order Chebychev polynomial function as background PDF. The obtained resolutions of mass difference at different Y masses are shown in Fig. 29. It varies from ∼1.7 MeV at Y mass of 4.15 GeV/c^2 to ∼5.5 MeV at Y mass of 4.75 GeV/c^2.

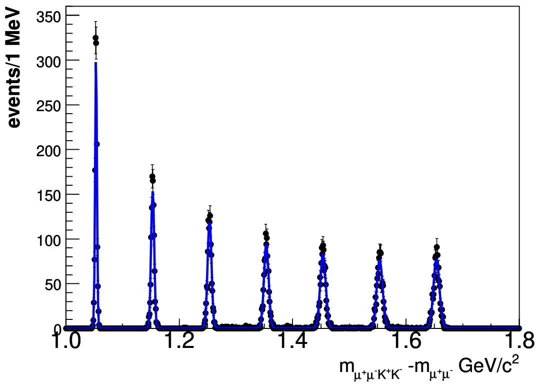

Figure 28: The mass difference between $J/\psi\phi$ and J/ψ in the MC $B \to YK^+, Y \to J/\psi\phi$ mass window after the basic cuts, L_{xy} and kaon LR cuts at the starting point.

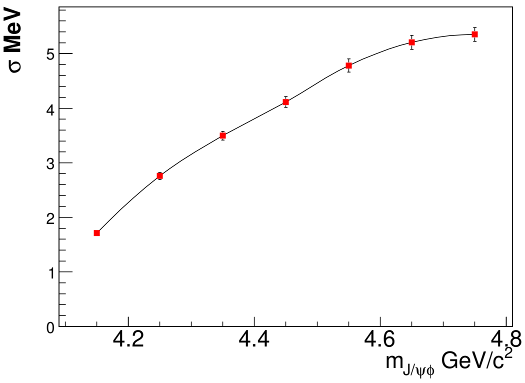

Figure 29: The resolutions for the mass difference between $J/\psi\phi$ and J/ψ as a function of $J/\psi\phi$ mass at CDF.

3.3 Justification of Minimum L_{xy} and Kaon LR

Due to the fact of not knowing precisely the mass and width of possible search object(s), it is not convenient to optimize a search object directly. The two main cuts (minimum L_{xy} and minimum Kaon LR) are justified by $S/\sqrt{S+B}$, where S represents the number of $B^+ \to J/\psi\phi K^+$ events in the mass range between 5.0 and 5.6 GeV/c^2 and B represents the number of background events in the same mass region. The choice of justifying $B^+ \to J/\psi\phi K^+$ is a comprise and we believe that it is sufficient to guarantee our cuts to be unbiased.

Since the PID simulation in MC is not well validated in data, the justification is done on data itself. For a choice of minimum L_{xy} and a minimum kaon LR, we do a unbinned log-likelihood fit to the mass distribution of $J/\psi\phi K^+$ to extract the number of $B^+ \to J/\psi\phi K^+$ (S) and the number of background (B) with B^+ mass constrained to its PDG value and width constrained to 5.9 MeV. The B^+ signal PDF is represented by a Gaussian function and the background shape is just a first-order Chebychev polynomial function. The lego plot of $S/\sqrt{S+B}$ as a function of minimum L_{xy} and minimum kaon LR (apply to all three kaons) is shown in Fig. 30. The justified minimum L_{xy} is 500 μm and the minimum kaon LR is 0.2 as shown in Fig. 30. The two cuts are controlled by this justification to be unbiased although it does not mean that they are optimized for our search objects and have the best sensitivities.

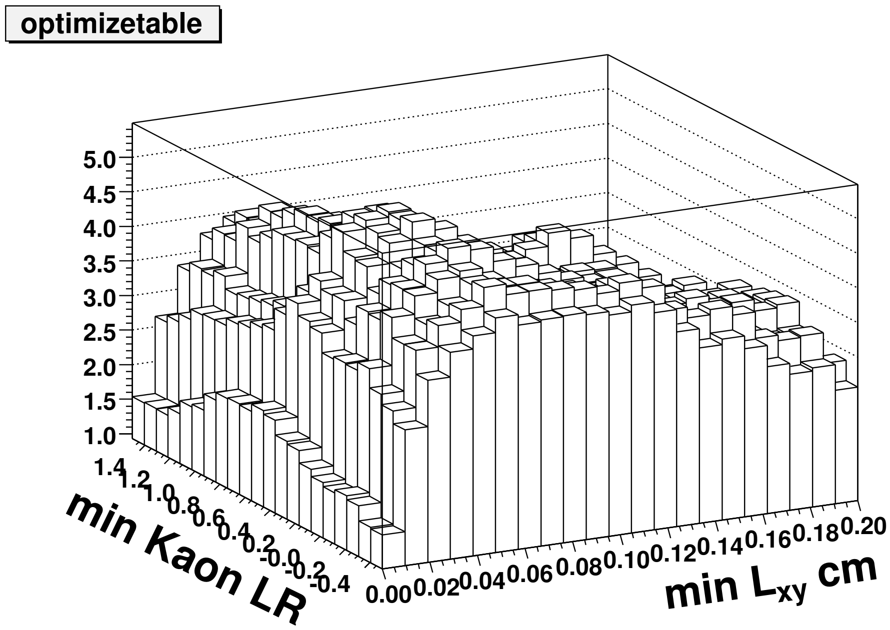

Figure 30: The $S/\sqrt{S+B}$ as a function of minimum L_{xy} and minimum kaon LR.

3.4 The $B^+ \to J/\psi\phi K^+$ Signal with the Justified Cuts

The invariant mass of $J/\psi\phi K^+$ after adding the basic cuts and the justified cuts ($L_{xy} > 500\mu$m and kaon LR > 0.2) are shown in Fig. 31. A unbinned log-likelihood fit with a Gaussian function as B^+ signal and a first-order Chebychev polynomial function as background return a yield of 78 ± 10, where the B^+ mass is fixed to its PDG value and its width is fixed to 5.9 MeV obtained from MC. The B^+ signal purity is greater than 80%. This is still the largest $B^+ \to J/\psi\phi K^+$ sample for a single channel in the world and we are going to search for structures in the $J/\psi\phi$ mass spectrum from the defined B mass window.

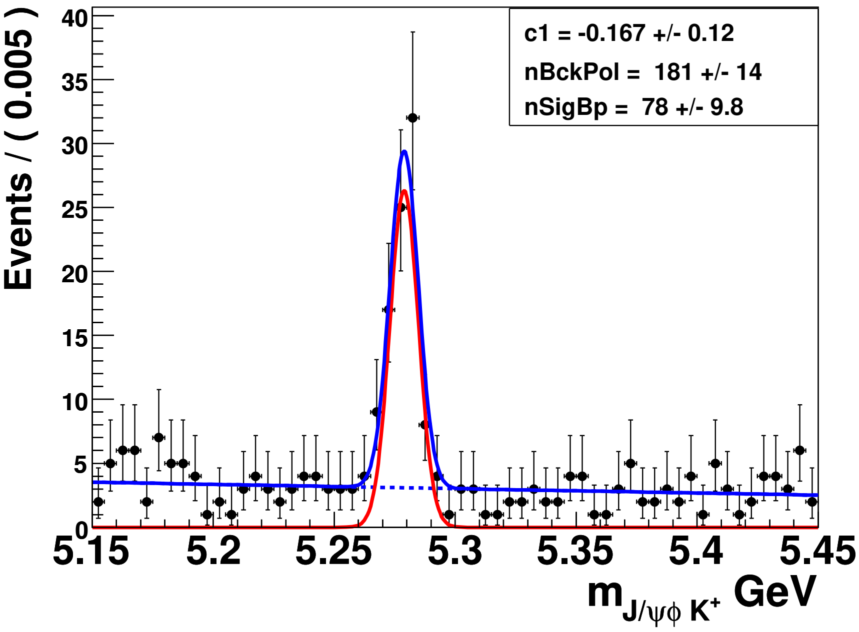

Figure 31: The $J/\psi\phi K^+$ mass with basic cuts, justified minimum L_{xy} and kaon LR.

3.5 Check with Generic B meson MC

Although we are searching structures through exclusive $B^+ \to J/\psi\phi K^+$ decays, we can still have other B contaminations under B^+ signal. To understand this systematically, we generated 10 million MC of generic $B^+/B^0/B_c/B_s$ events including a $J/\psi \to \mu^+\mu^-$ in the final state by the B meson decay table from B factories. The reconstructed $B^+ \to J/\psi\phi K^+$ mass from these generic B MC after applying the basic cuts, justified L_{xy} and kaon LR are shown in Fig. 32, 33, 34, 35. The mass difference between $J/\psi\phi$ and J/ψ in the defined B^+ mass window are shown in Fig. 36, 37, 38, 39. The contamination we need to worry about is from B_s decays and it turns out that it is due to K/π mis-identification of $B_s \to \psi(2S)\phi, \psi(2S) \to J/\psi\pi^+\pi^-$ channel. We will discuss this further in next chapter.

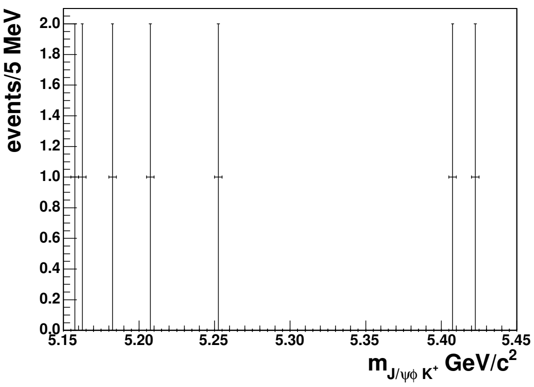

Figure 32: The $J/\psi\phi K^+$ mass from generic $B^+ \to J/\psi + X$ MC after applying the justified cuts and basic cuts.

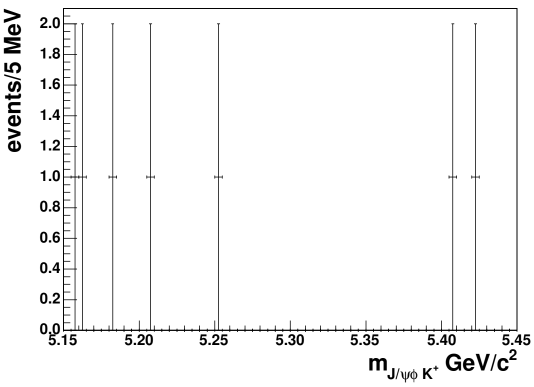

Figure 33: The $J/\psi\phi K^+$ mass from generic $B^0 \to J/\psi + X$ MC after applying the justified cuts and basic cuts.

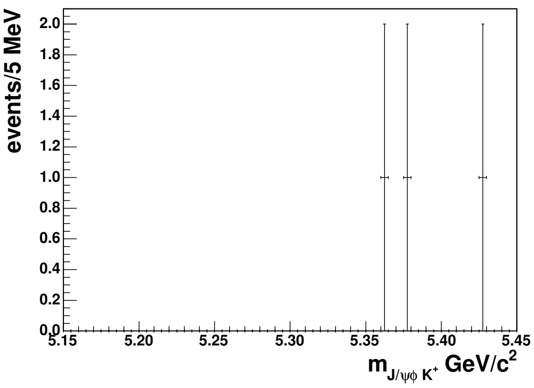

Figure 34: The $J/\psi\phi K^+$ mass from generic $B_c \to J/\psi + X$ MC after applying the justified cuts and basic cuts.

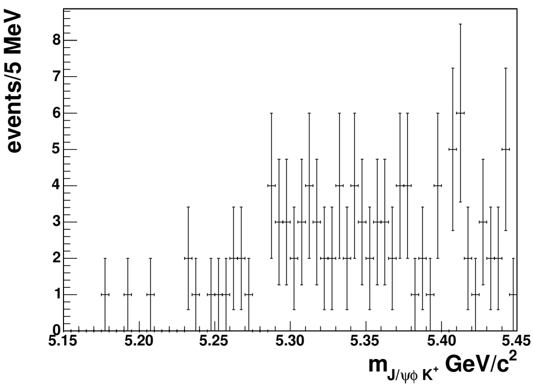

Figure 35: The $J/\psi\phi K^+$ mass from generic $B_s \to J/\psi + X$ MC after applying the justified cuts and basic cuts.

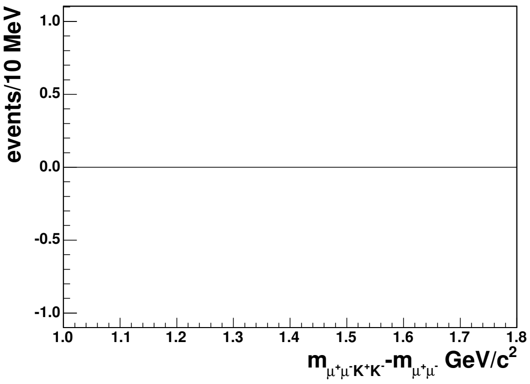

Figure 36: The mass difference between $J/\psi\phi$ and J/ψ in the defined B mass window from generic $B^+ \to J/\psi + X$ MC after applying the justified cuts and basic cuts.

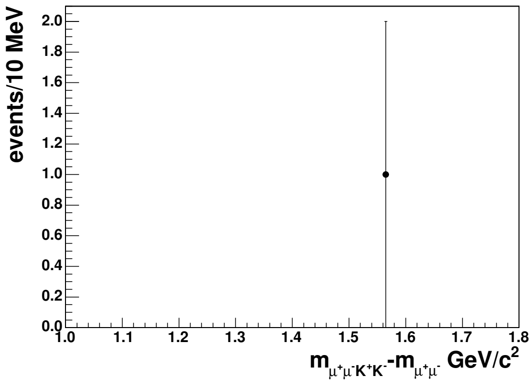

Figure 37: The mass difference between $J/\psi\phi$ and J/ψ in the defined B mass window from generic $B^0 \to J/\psi + X$ MC after applying the justified cuts and basic cuts.

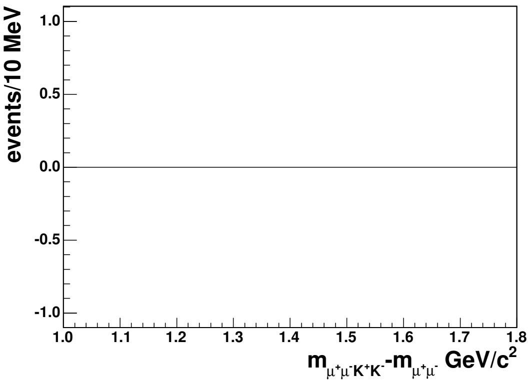

Figure 38: The mass difference between $J/\psi\phi$ and J/ψ in the defined B mass window from generic $B_c \to J/\psi + X$ MC after applying the justified cuts and basic cuts.

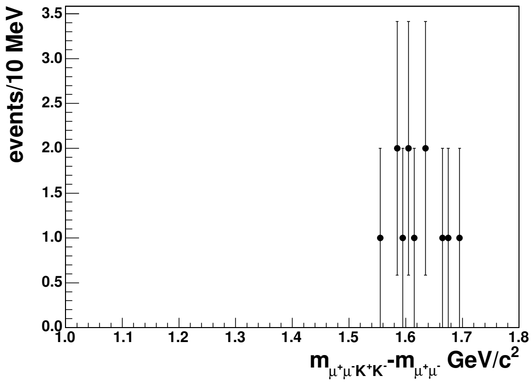

Figure 39: The mass difference between $J/\psi\phi$ and J/ψ in the defined B mass window from generic $B_s \to J/\psi + X$ MC after applying the justified cuts and basic cuts .

4 B_s Contamination and Other MC Studies

4.1 More B_s MC Studies

As shown in the last chapter, we do have contamination from $B_s \to \psi(2S)\phi, \psi(2S) \to J/\psi\pi^+\pi^-, J/\psi \to \mu^+\mu^-$ decays. We generated 5 million MC events for this channel and the invariant mass of $J/\psi\phi K^+$ after applying the basic cuts, $L_{xy} > 500$ μm and kaon LR > 0.2 (the justified cuts) is shown in Fig. 40, and the mass difference between $J/\psi\phi$ and J/ψ in the defined B mass window is shown in Fig. 41. A fit with a Novosibirsk function [8] returns a mass peak of 1.650 ± 0.005 GeV/c^2, a width of 37.3 ± 2.6 MeV and a tail of -0.383 ± 0.073. We will fix these parameters when we fit to the mass difference between $J/\psi\phi$ and J/ψ in the data.

The Dalitz plots [9] in the defined B mass window for the B_s contamination are shown in Fig. 42 and 43, they concentrate at the right-bottom corner.

[8] The Novosibirsk function is usually defined by: $f(m_{ES}) = A_S \times \exp(-0.5\ln^2[1 + \Lambda\tau \cdot (m_{ES} - m_0)]/\tau^2 + \tau^2)$, where $\Lambda = \sinh(\tau\sqrt{\ln 4})/(\sigma\tau\sqrt{\ln 4})$, the peak position is m_0, the width is σ, and τ is the tail parameter.

[9] The $J/\psi\phi$ mass is calculated as $(m_{\mu^+\mu^-K^+K^-} - m_{\mu^+\mu^-} + 3.0967)$ and $J/\psi K^+$ mass is calculated as $(m_{\mu^+\mu^-K^+} - m_{\mu^+\mu^-} + 3.0967)$.

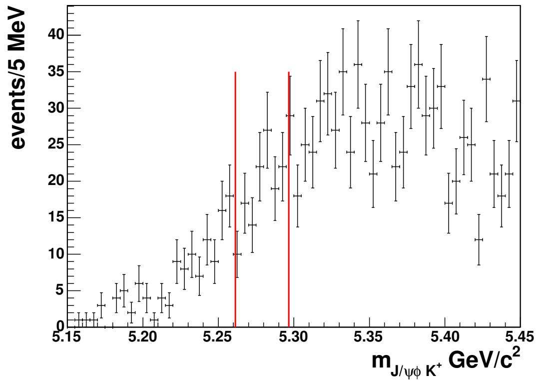

Figure 40: The invariant mass of $J/\psi\phi K^+$ from $B_s \to \psi(2S)\phi, \psi(2S) \to J/\psi\pi^+\pi^-$ MC after applying the basic cuts, justified L_{xy} and kaon LR.

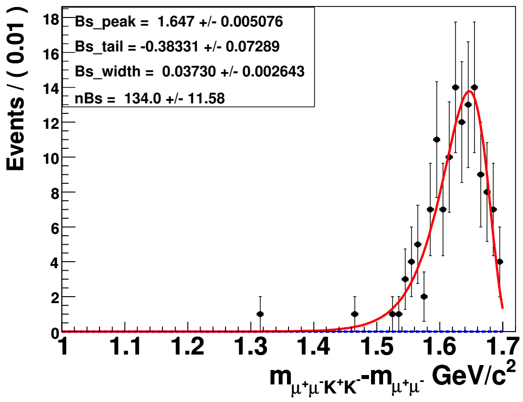

Figure 41: The mass difference between $J/\psi\phi$ and J/ψ in the define B Mass window from $B_s \to \psi(2S)\phi, \psi(2S) \to J/\psi\pi^+\pi^-$ MC after applying the basic cuts, justified L_{xy} and kaon LR.

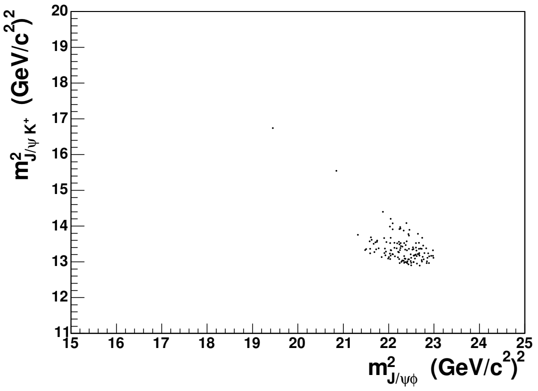

Figure 42: The Dalitz plot ($m^2_{J/\psi\phi}$ vs $m^2_{J/\psi K^+}$) from $B_s \to \psi(2S)\phi, \psi(2S) \to J/\psi\pi^+\pi^-$ MC after applying the basic cuts, justified L_{xy} and kaon LR.

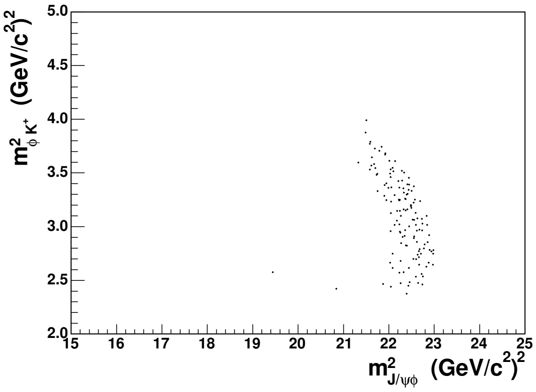

Figure 43: The Dalitz plot ($m^2_{J/\psi\phi}$ vs $m^2_{\phi K^+}$) from $B_s \to \psi(2S)\phi, \psi(2S) \to J/\psi\pi^+\pi^-$ MC after applying the basic cuts, justified L_{xy} and kaon LR.

4.2 Dalitz Plots from MC

Fig. 44 to 47 show the Dalitz plots after we apply the basic cuts, justified L_{xy} and kaon LR for the MC samples of $B^+ \to J/\psi\phi K^+$ generated in phase space and $B^+ \to YK^+, Y \to J/\psi\phi$ where the widths of Y were set be zero and the masses of Y were set to be the following values: 4.15, 4.25, 4.35, 4.45, 4.55, 4.65, 4.75 GeV/c^2. There is no structure in Fig. 44 and 45 as expected and seven bands in Fig. 46 and 47 as we set.

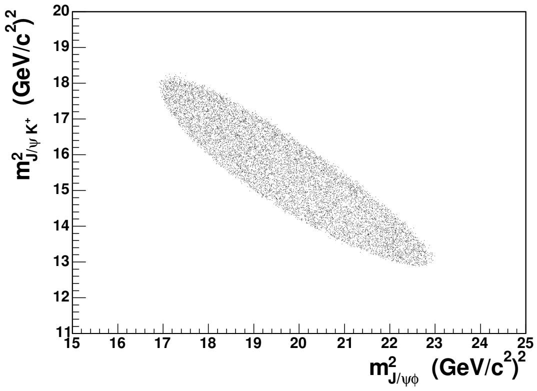

Figure 44: The Dalitz plot ($m^2_{J/\psi\phi}$ vs $m^2_{J/\psi K^+}$) from $B^+ \to J/\psi\phi K^+$ MC generated in phase space.

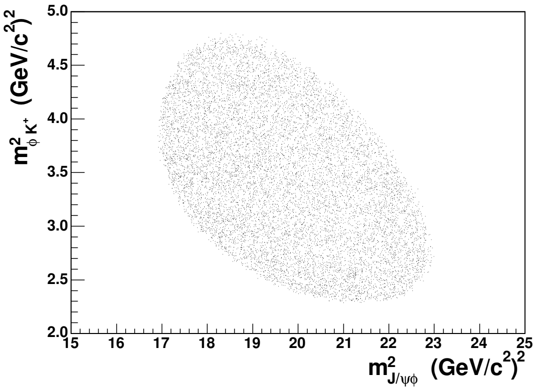

Figure 45: The Dalitz plot ($m^2_{J/\psi\phi}$ vs $m^2_{\phi K^+}$) from $B^+ \to J/\psi\phi K^+$ MC generated in phase space.

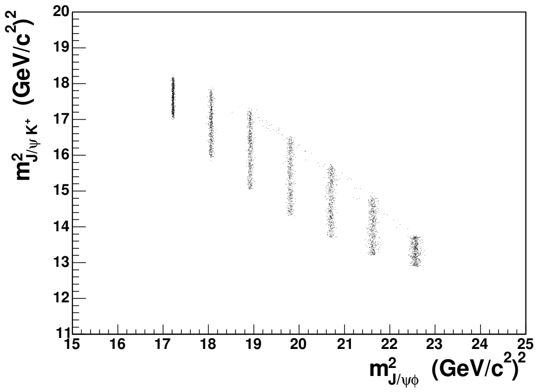

Figure 46: The Dalitz plot ($m^2_{J/\psi\phi}$ vs $m^2_{J/\psi K^+}$) from $B^+ \to YK^+, Y \to J/\psi\phi$ MC.

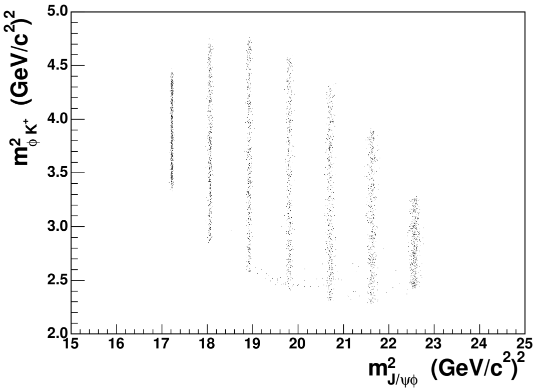

Figure 47: The Dalitz plot ($m^2_{J/\psi\phi}$ vs $m^2_{\phi K^+}$) from $B^+ \to YK^+, Y \to J/\psi\phi$ MC.

4.3 Proposal for Significance Estimation

We propose to use the unbinned log-likelihood ratio of $-2\log(\mathrm{L}_{\mathrm{max}}/\mathrm{L}_0)$ between signal and null hypothesis fit to calculate the p value and further estimate the significance based on the p value. Since we do not know the mass and width precisely, we take the d.o.f as 3 to calculate the p value.

5 Search for Structures in the $J/\psi\phi$ Spectrum

5.1 The $J/\psi\phi$ Spectrum

As shown in Fig. 48, we define the B^+ mass window as within 3 σ of its PDG value where we take σ as 5.9 MeV obtained from MC. We further define a high-sideband as in the $J/\psi\phi K^+$ mass range between 6 and 9 σ of B^+'s PDG value, and a low-sideband as in the $J/\psi\phi K^+$ mass range between -6 and -9 σ of B^+'s PDG value. The sum of low-sideband and high-sideband is the total sidebands. This is a reasonable choice assuming a linear background shape in the mass distribution of $J/\psi\phi K^+$.

The Dalitz plots in the B mass window are shown in Fig. 49 and 50, there seems a band in the up-left corner. The projections in the mass difference between $J/\psi\phi$ and J/ψ in the B mass window (black) and in the sidebands (red) are shown in Fig. 51, 52 (zoom). We see a peak around the $J/\psi\phi$ threshold in the B mass window but not in the B sidebands.

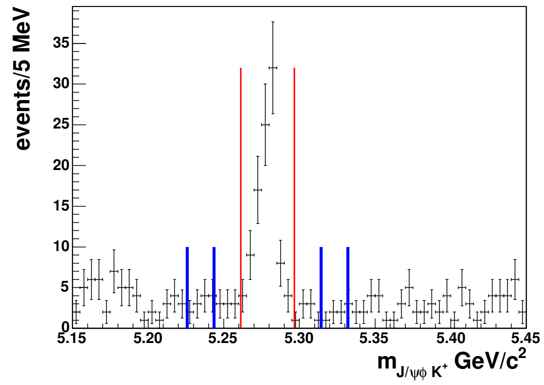

Figure 48: The invariant mass of $J/\psi\phi K^+$ in data with basic cuts, justified L_{xy} and kaon LR.

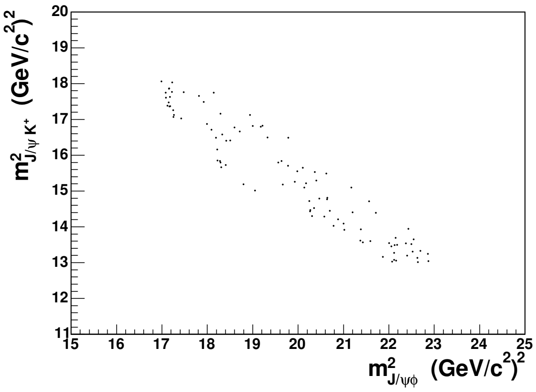

Figure 49: The Dalitz plot in the defined B mass window in data with basic cuts, justified L_{xy} and kaon LR.

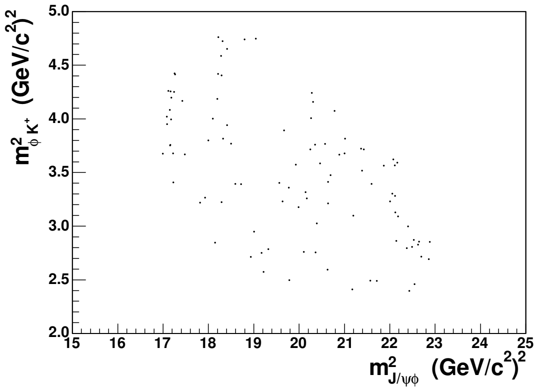

Figure 50: The Dalitz plot in the defined B mass window in data with basic cuts, justified L_{xy} and kaon LR.

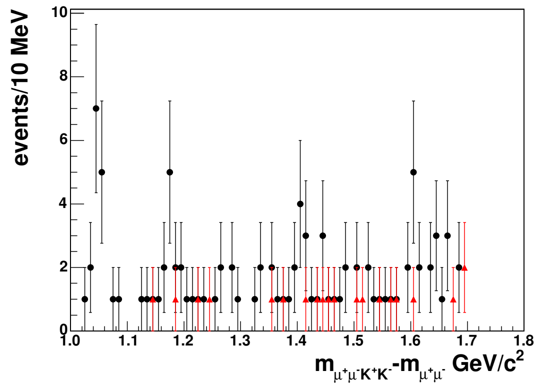

Figure 51: The mass difference between $J/\psi\phi$ and J/ψ in the defined B mass window in data with basic cuts, justified L_{xy} and kaon LR. The red histogram is from B sidebands.

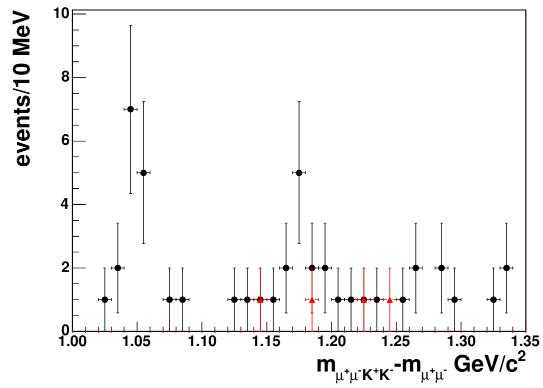

Figure 52: The Zoomed mass difference between $J/\psi\phi$ and J/ψ in the defined B mass window in data with basic cuts, justified L_{xy} and kaon LR. The red histogram is from B sidebands.

5.2 Cross Check

As a cross check, we vary one of the main cuts at one time to investigate the mass difference between $J/\psi\phi$ and J/ψ in the defined B mass window. We see reasonable peaks in the mass difference spectrum as shown below.

5.2.1 Varying L_{xy} (Default value: 500 μm)

The invariant mass of $J/\psi\phi K^+$ and the mass difference between $J/\psi\phi$ and J/ψ in the defined B mass window are shown in Fig. 53, 54 for minimum L_{xy} of 400 μm and Fig. 55, 56 for minimum L_{xy} of 600 μm.

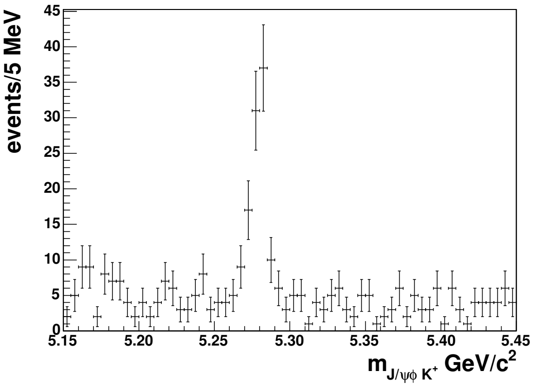

Figure 53: The invariant mass of $J/\psi\phi K^+$ in data with $L_{xy} > 400\mu$m.

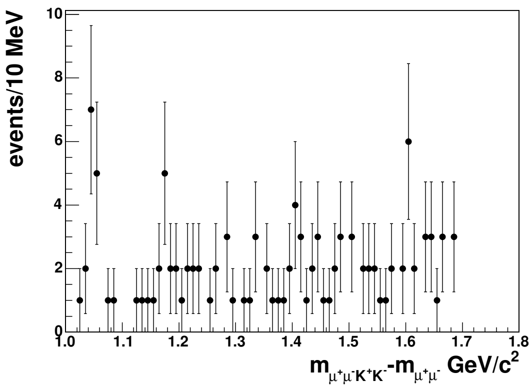

Figure 54: The mass difference between $J/\psi\phi$ and J/ψ in the defined B mass window in data with $L_{xy} > 400\mu$m.

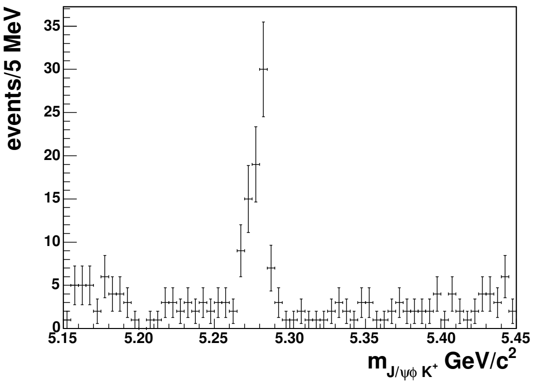

Figure 55: The invariant mass of $J/\psi\phi K^+$ in data with $L_{xy} > 600\mu$m.

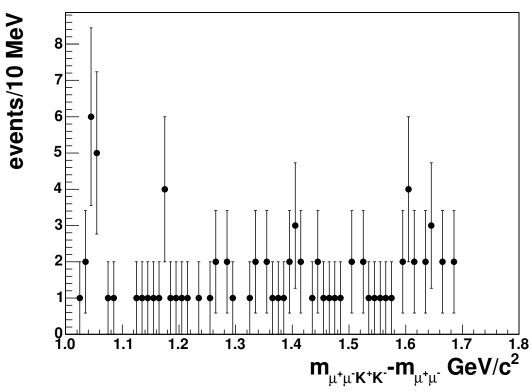

Figure 56: The mass difference between $J/\psi\phi$ and J/ψ in the defined B mass window in data with $L_{xy} > 600\mu$m.

5.2.2 Varying Kaon LR (default value: 0.2)

The invariant mass of $J/\psi\phi K^+$ and the mass difference between $J/\psi\phi$ and J/ψ in the defined B mass window are shown in Fig. 57, 58 for minimum kaon LR (all three kaons) of 0.0 and Fig. 59, 60 for minimum kaon LR (all three kaons) of 0.4.

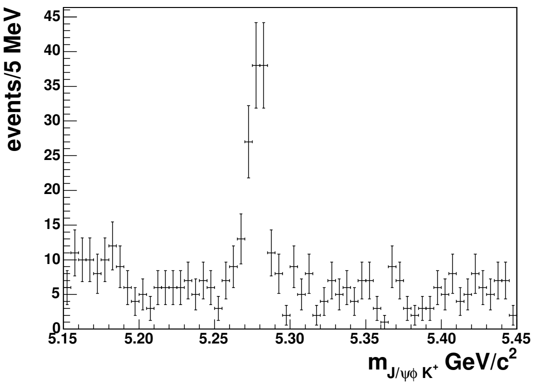

Figure 57: The invariant mass of $J/\psi\phi K^+$ in data with kaon LR > 0.0.

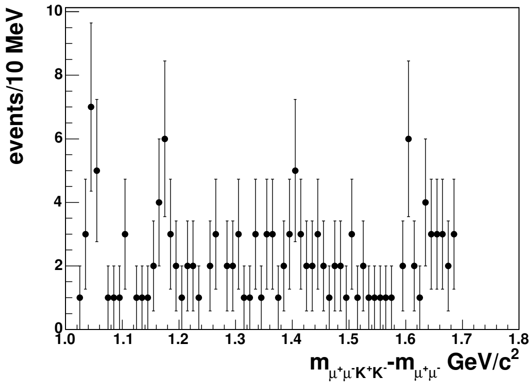

Figure 58: The mass difference between $J/\psi\phi$ and J/ψ in the defined B mass window in data with kaon LR > 0.0.

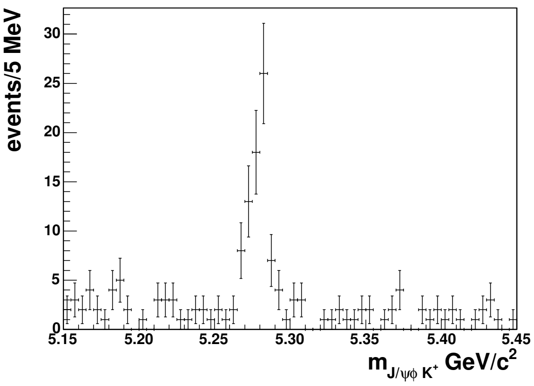

Figure 59: The invariant mass of $J/\psi\phi K^+$ in data with kaon LR > 0.4.

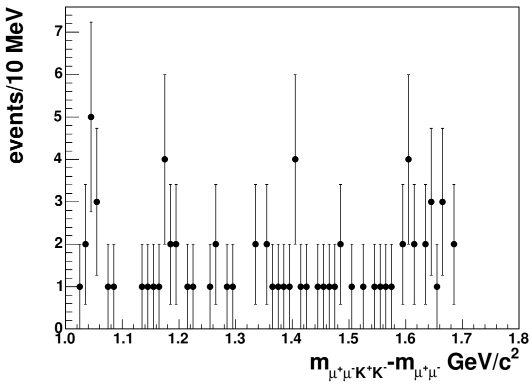

Figure 60: The mass difference between $J/\psi\phi$ and J/ψ in the defined B mass window in data with kaon LR > 0.4.

5.2.3 Tightening Muon Selection (default: CMP/CMU/CMX)

The invariant mass of $J/\psi\phi K^+$ and the mass difference between $J/\psi\phi$ and J/ψ in the defined B mass window by removing CMX muons are shown in Fig. 61, 62.

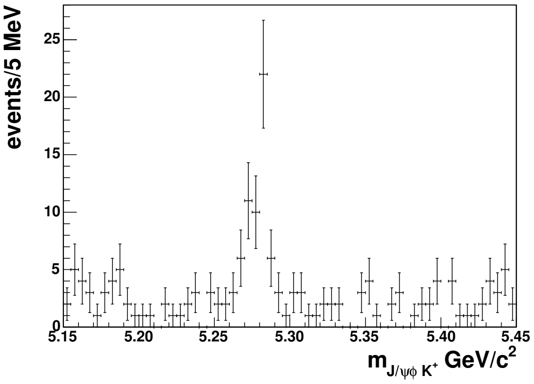

Figure 61: The invariant mass of $J/\psi\phi K^+$ in data with muon hits on CPU or CMP.

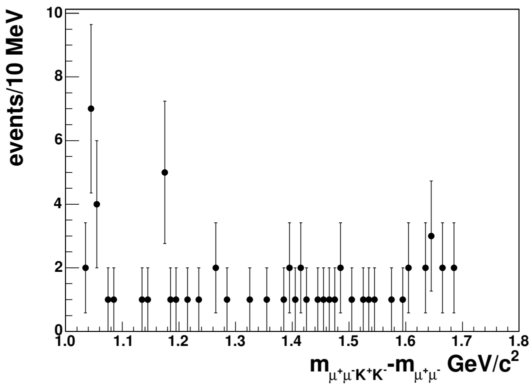

Figure 62: The mass difference between $J/\psi\phi$ and J/ψ in the defined B mass window in data with CPU or CMP muons.

5.2.4 Varying B mass window (default: within 3 σ)

The mass difference between $J/\psi\phi$ and J/ψ within 1 σ and 5 σ of the nominal B mass are shown in Fig. 63, 64.

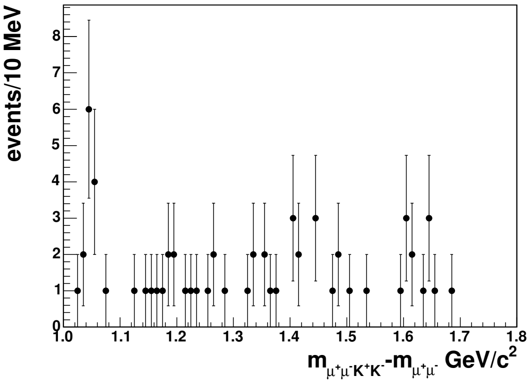

Figure 63: The mass difference between $J/\psi\phi$ and J/ψ within 1 σ of nominal B mass.

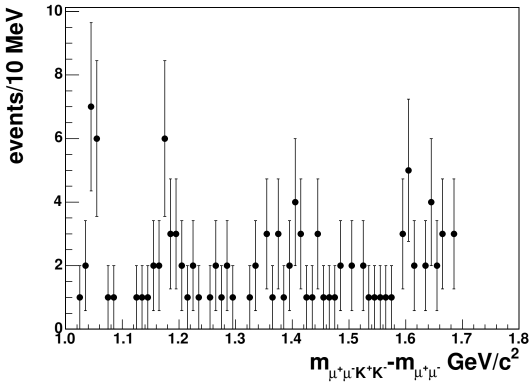

Figure 64: The mass difference between $J/\psi\phi$ and J/ψ within 5 σ of nominal B mass.

5.2.5 Candidates per Event

We keep all possible candidates satisfying requirements per event to avoid bias. The run number distribution for those events in the defined B mass window is shown in Fig. 65 and it shows that more than 95% of the runs only contribute 1 candidate.

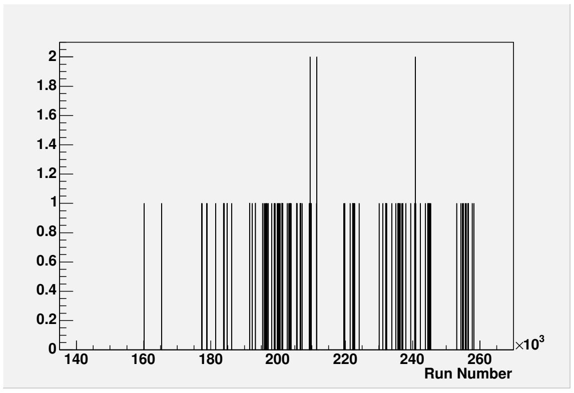

Figure 65: The run number distribution for those events in the defined B mass window.

5.3 Background Subtraction using sPlot Technique

We use the sPlot technique [24] to subtract non-B backgrounds. The sPlot technique assigns to each event a weight for each possible category to which it might belong. These weights depend on a collection of observables. It is then possible to plot the distribution for an additional variable that is not correlated with the variables used to assign the weights. Asymptotically this technique gives the true distribution. In our case, we obtain the sWeight from the fit to the $J/\psi\phi K^+$ mass for $B^+ \to J/\psi\phi K^+$ category or background category. The projection of the mass difference between $J/\psi\phi$ and J/ψ for $B^+ \to J/\psi\phi K^+$ component (category) shown in Fig. 66. Fig. 67 shows the projections of mass difference between $J/\psi\phi$ and J/ψ for the $B^+ \to J/\psi\phi K^+$ component and background component, where each projection is normalized to the number of events in the defined B mass window. The projections from B signal and background demonstrate that the structure at the $J/\psi\phi$ threshold is from B signal.

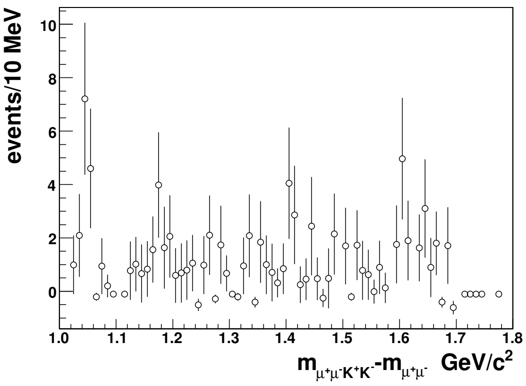

Figure 66: The sWeighted mass difference between $J/\psi\phi$ and J/ψ from B^+ in data with basic cuts, justified L_{xy} and kaon LR.

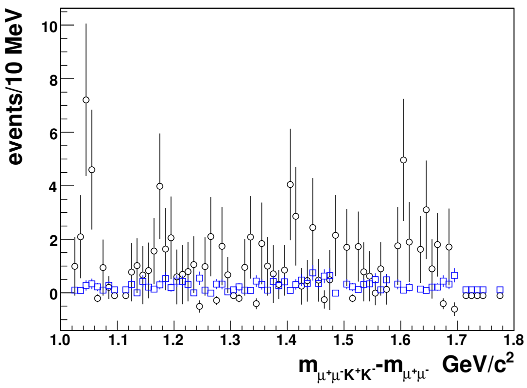

Figure 67: The sWeighted mass difference between $J/\psi\phi$ and J/ψ from B^+ and non-B^+ background in data with basic cuts, justified L_{xy} and kaon LR. They are normalized to the number of events in the defined B mass window.

5.4 Fit to the Mass Difference and Significance Calculation

We use a simple Breit-Wigner (non-relativistic) function convoluted with a Gaussian resolution function (set to be 1.7 MeV obtained from MC) to represent the peak at the threshold. We use the following threshold function to model the background: $q(Q^{1/2} + a_1 Q^{3/2})$ where q is the momentum of J/ψ in the rest frame of $J/\psi\phi$, $Q = \Delta m_{max} - \Delta m$ and $\Delta m_{max} = 1.69$ GeV/c^2. The contamination from $B_s \to \psi(2S)\phi, \psi(2S) \to J/\psi\pi^+\pi^-$ is modeled by a Novosibirsk function and we fix its parameters to the values obtained from MC. The signal (with PDF for the peak at the threshold) and null (without PDF for the peak at the threshold) hypotheses unbinned log-likelihood fit to the mass difference between $J/\psi\phi$ and J/ψ in the defined B mass window are shown in Fig. 68, 69. The signal hypotheses fit returns a mass difference of 1046.9 ± 2.4 MeV/c^2, a width of 11.3 ± 4.7 MeV and a yield of 15 ± 4. The fit also returns other free parameters: number of background as 67 ± 10, number of contaminated B_s as 16 ± 7 and a_1 as 3.043 ± 4.464.

The log-likelihood difference between signal $2 \times \log(\mathrm{L_{max}})$ and null $2 \times \log(\mathrm{L_0})$ hypotheses is 48.4. We take d.o.f as 3 since we do not know the mass and width precisely and the p value is 1.8×10^{-10} which corresponds to a significance of 6.3 σ.

We use the background shape from the fit to generate 82 events, and then add 16 events from the Novosibirsk function as B_s contamination. We then repeat the fitting process as in the data to extract "signal" which is bigger or equal to the effect in the data. We tried 2.4 million Toy MC experiments and we did not see fluctuation effect bigger than the effect in the data.

Assume the same signal selection efficiency (not quite true) between $B^+ \to J/\psi\phi K^+$ and $B^+ \to YK^+, Y \to J/\psi\phi$ and ignore the B/Y polarization, the BF ratio of $\beta(B^+ \to YK^+) \times \beta(Y \to J/\psi\phi)/\beta(B^+ \to J/\psi\phi K^+)$ is about 19%. Taking BF of $B^+ \to J/\psi\phi K^+$ as 5.2×10^{-5}, the BF of $B^+ \to YK^+, Y \to J/\psi\phi$ is at the level between 10^{-6} and 10^{-5}.

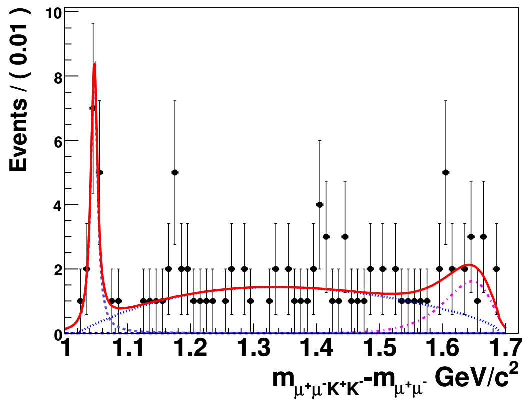

Figure 68: The signal hypothesis fit to the mass difference between $J/\psi\phi$ and J/ψ in the defined B mass window.

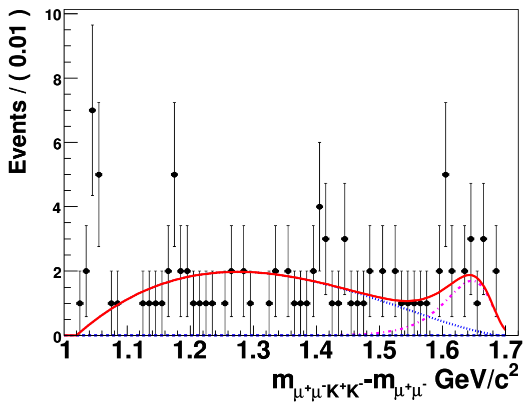

Figure 69: The null hypothesis fit to the mass difference between $J/\psi\phi$ and J/ψ in the defined B mass window.

To study the effect of background shape on signal significance, we re-do unbinned log-likelihood signal and null hypotheses fit to the mass difference assuming different background shapes and changing the end points in the threshold background function by the ϕ mass window (7 MeV/c^2). We also tried to keep only one candidate per event in the $J/\psi\phi K^+$ mass range from 5.0 to 5.6 GeV/c^2 by selecting a candidate with the highest vertex probability if there are multiple candidates for one event. The returned $2 \times \log(\mathrm{L}_{\mathrm{max}}/\mathrm{L}_0)$ and significance are shown in Table 1, they are all beyond 5 σ. The signal and null hypotheses fit with one candidate per event, and different end points are shown in Fig. 70, 71, 72, 73, 74, 75.

Table 1: The returned $2 \times \log(\mathrm{L}_{\mathrm{max}}/\mathrm{L}_0)$ from the fit to the mass difference between $J/\psi\phi$ and J/ψ with different background assumptions, one candidate per event and varied end points.

Background shape	$2 \times \log(\mathrm{L}_{\mathrm{max}}/\mathrm{L}_0)$	Significance
One candidate per event	42.4	5.9 σ
Higher end point	77.6	8.3 σ
Lower end point	42.4	5.9 σ
Gaussian background	42.2	5.9 σ
$q^3(Q^{1/2} + a_1 Q^{3/2})$	196.6	>10 σ

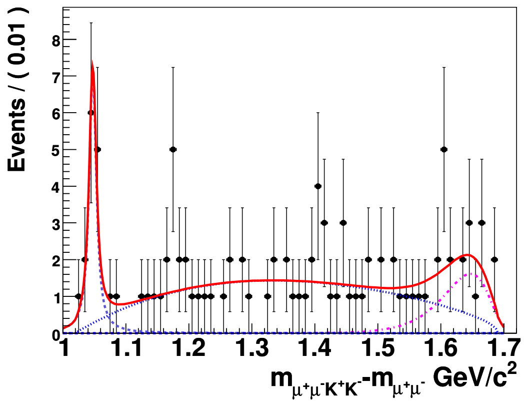

Figure 70: The signal hypothesis fit to the mass difference between $J/\psi\phi$ and J/ψ in the defined B mass window with one candidate per event.

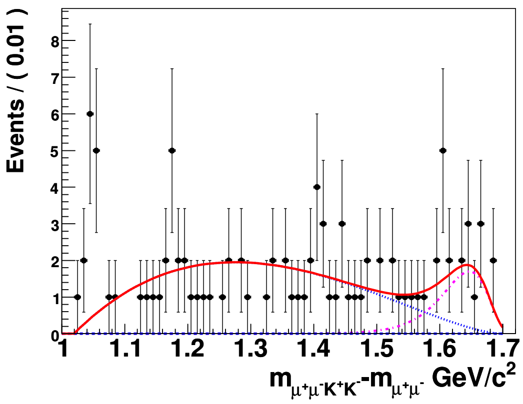

Figure 71: The null hypothesis fit to the mass difference between $J/\psi\phi$ and J/ψ in the defined B mass window with one candidate per event.

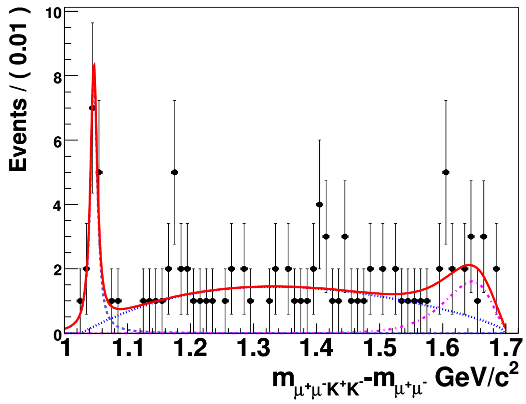

Figure 72: The signal hypothesis fit to the mass difference between $J/\psi\phi$ and J/ψ in the defined B mass window with higher end point.

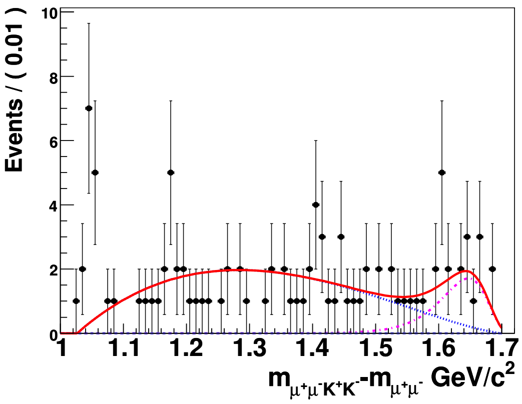

Figure 73: The null hypothesis fit to the mass difference between $J/\psi\phi$ and J/ψ in the defined B mass window with higher end point.

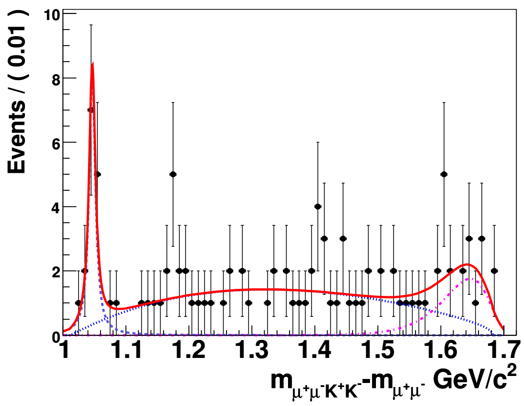

Figure 74: The signal hypothesis fit to the mass difference between $J/\psi\phi$ and J/ψ in the defined B mass window with lower end point.

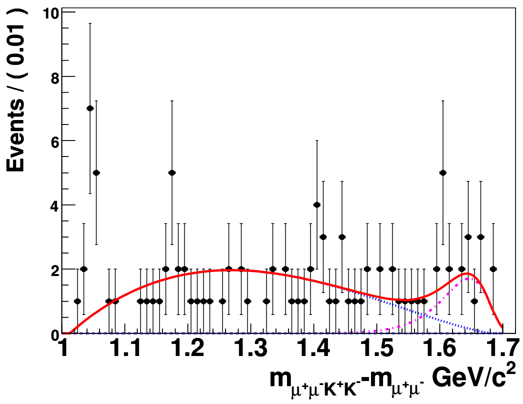

Figure 75: The null hypothesis fit to the mass difference between $J/\psi\phi$ and J/ψ in the defined B mass window with lower end point.

5.5 Cross Check of Background Shape and Significance

In order to check the validation of background shape and the significance estimation, we loose the cuts to allow more background for better statistics [10]. We use the following relaxed cuts to replace the previous cuts: $L_{xy} > 250$ μm, kaon logged LR > 0.0, minimum $r - \phi$ silicon hit on each track to be 3, vertex fit χ^2 probability to be greater than 10^{-5}. The mass difference between $J/\psi\phi$ and J/ψ in the defined B mass window using the above relaxed cuts is shown in Fig. 76. We just use the same background function $q(Q^{1/2} + a_1 Q^{3/2})$ to fit to the mass difference as shown in Fig. 76. We assume all events as background and the fit is a binned χ^2 fit. However, the fit barely converged (converge status is OK) and returned a_1 as 0.71 ± 0.35. It seems a reasonable background modeling. The signal and null hypothesis fit to the mass difference are shown in Fig. 77 and 78. The signal fit returns a yield of 35 ± 7, a mass difference of 1045.0 ± 1.7 MeV/c^2 and a width of 11.6 ± 3.7 MeV. Other parameters returned are: number of background to be 472 ± 25, number of B_s contamination to be 33 ± 14 and a_1 to be 1.60 ± 0.91. The returned $2 \times \log(\mathrm{L_{max}}/\mathrm{L_0})$ is 117.4, which is about 10 σ. We also investigate the expected efficiency increase for relaxed cuts from control samples. We expect the following efficiency changes: $0.56 \to 0.67$ (Fig. 15) due to L_{xy} relaxing, $0.52 \to 0.64$ (Fig. 5) due to kaon PID LR relaxing for the two kaons from ϕ decay, $0.75 \to 0.84$ (Fig. 16) due to kaon PID LR relaxing for the kaon from B decay, increase of 43% for Vertex Probaility relaxing and SVX relaxing based on $B_s \to J/\psi\phi$ control sample, 4.1% increase due to SVX relaxing on the kaon track from B decays based on $B^+ \to J/\psi K^+$ control sample. Put these together, we expect the number of signal increase from 15 to 37, and we obtain 35 ± 7 events from the fit. That is to say, the signal yield obtained from cut relaxing is consistent with expectation of efficiency increase.

[10] This was suggested by multiple people

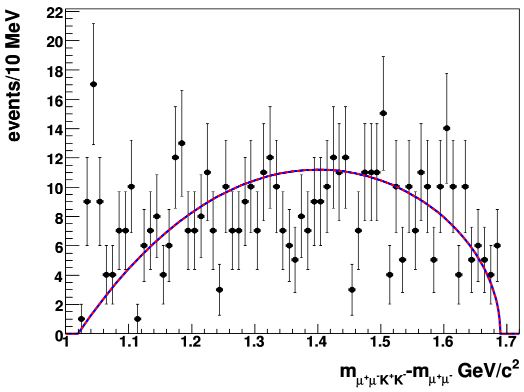

Figure 76: The χ^2 background shape fit to the mass difference between $J/\psi\phi$ and J/ψ in the defined B mass window with relaxed cuts.

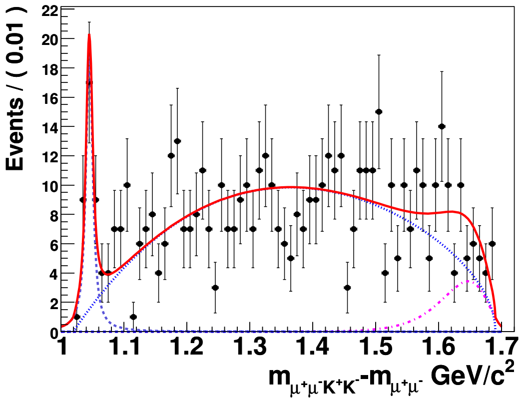

Figure 77: The signal hypothesis fit to the mass difference between $J/\psi\phi$ and J/ψ in the defined B mass window with relaxed cuts.

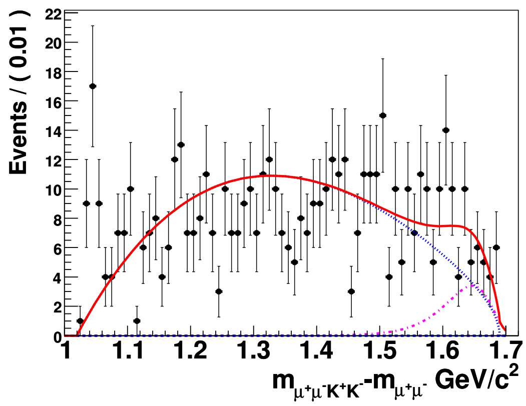

Figure 78: The null hypothesis fit to the mass difference between $J/\psi\phi$ and J/ψ in the defined B mass window with relaxed cuts.

5.6 Cross Check of Possible Structures at ϕK^+ Mass Spectrum

The ϕK^+ mass distribution for those events with the mass difference between $J/\psi\phi$ and J/ψ to be less than 1.1 GeV/c^2 is shown in Fig. 79. There is no structures shown in this plot. However, we can not exclude the possibility that known or unknown charged $K^* \to \phi K^+$s produce bumps at other positions due to interference effect. It is very difficult to draw conclusion due to low statistics.

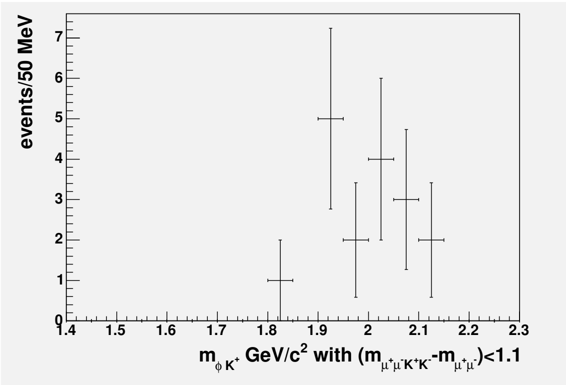

Figure 79: The mass distribution of ϕK^+ for those events with the mass difference between $J/\psi\phi$ and J/ψ to be less than 1.1 GeV/c^2.

5.7 Systematics and the Results of Mass and Width

In order to study the systematics of the mass and the width of the structure at $J/\psi\phi$ threshold, we re-do a unbinned log-likelihood fit to the mass difference between $J/\psi\phi$ and J/ψ in the defined B mass window by varying the cuts/mass resolution and assuming different background shapes. The returned mass differences and widths from the fit are shown in Table 2.

Table 2: The returned parameters from the fit to the mass difference between $J/\psi\phi$ and J/ψ with different cuts, mass resolution and background assumptions.

Cuts or background shape	Mass (MeV/c^2)	Width (MeV)
$L_{xy} > 400\mu$m	1046.8 ± 2.3	11.1 ± 4.8
$L_{xy} > 600\mu$m	1047.8 ± 2.4	11.4 ± 5.0
Kaon LR > 0.0	1045.8 ± 2.4	11.1 ± 4.8
Kaon LR > 0.4	1044.1 ± 2.7	11.2 ± 5.9
CMP or CMU	1046.5 ± 2.0	9.1 ± 4.3
Mass resolution of 3.4 MeV/c^2	1047.1 ± 2.5	9.5 ± 4.6
One candidate per event	1047.4 ± 2.8	12.6 ± 5.3
Higher end point	1046.8 ± 2.4	11.6 ± 4.8
Lower end point	1046.9 ± 2.4	10.9 ± 4.8
Gaussian background	1047.0 ± 2.4	10.9 ± 5.0
Threshold function $q^3(Q^{1/2} + a_1 Q^{3/2})$	1047.9 ± 2.8	17.4 ± 7.3

Since it is difficult to disentangle systematical uncertainty from statistical uncertainty with low statistical sample by varying the cuts, we skip those cases with varied cuts. The biggest variation for mass difference is 1.0 MeV/c^2 and the biggest variation for width is 6.1 MeV from the remaining cases. To be conservative, we assign 1.0 MeV/c^2 as the mass difference systematical uncertainty and 6.1 MeV as the width systematical uncertainty.

The mass difference for the structure at $J/\psi\phi$ threshold between $J/\psi\phi$ and J/ψ including systematics is 1046.3 ± 2.9(stat) ± 1.2(syst) MeV/c^2. By adding the J/ψ mass from PDG, we obtain the mass of the structure as: 4143.0 ± 2.9(stat)± 1.2(syst) MeV/c^2. The width of this structure including systematics is $11.7^{+8.3}_{-5.0}$(stat) ± 3.7(syst) MeV/c^2. Due to the fact that both J/ψ and ϕ are 1^{--} objects, the C parity of this structure is positive, other quantum numbers remains unknown.

5.8 The Significance of the Second and Third Peaks

As requested in the pre-bless meeting, we estimate the significance of the possible second and third peaks by the log-likelihood ratio between signal and null hypothesis fit. The signal and null hypothesis fits by assuming one and two more peaks are shown in Fig. 80, 81, 82, 83. The significance of the peak around 1.17 GeV is about 2.6 σ and the peak around 1.4 GeV is about 1.6 σ. The signal fit returns a yield of 11 ± 5, a mass difference of 1178.0 ± 3.7 MeV/c^2 and a width of 14 ± 11 MeV for the second peak; a yield of 7 ± 6, a mass difference of 1409.0 ± 6.5 MeV/c^2 and a width of 16 ± 25 for the third peak.

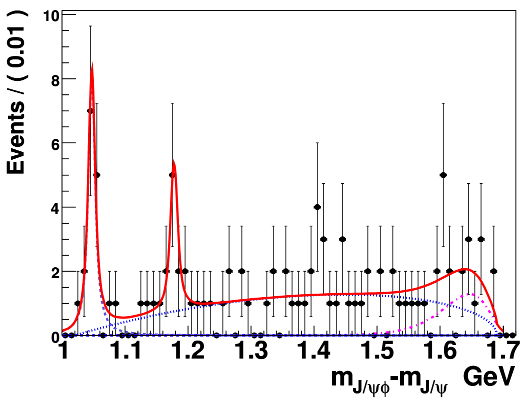

Figure 80: The signal hypothesis fit to the mass difference between $J/\psi\phi$ and J/ψ in the defined B mass window assuming a signal around the mass difference of 1.17 GeV.

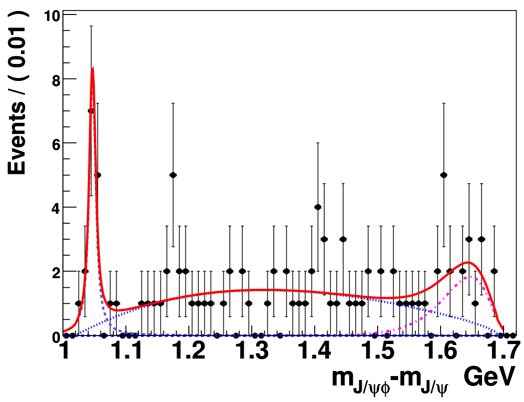

Figure 81: The null hypothesis fit to the mass difference between $J/\psi\phi$ and J/ψ in the defined B mass window assuming zero signal around the mass difference of 1.17 GeV.

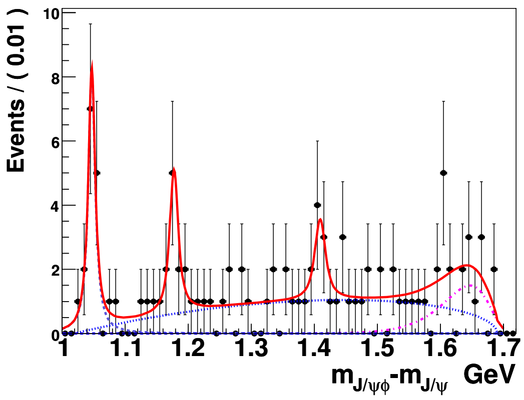

Figure 82: The signal hypothesis fit to the mass difference between $J/\psi\phi$ and J/ψ in the defined B mass window assuming a signal around the mass difference of 1.4 GeV.

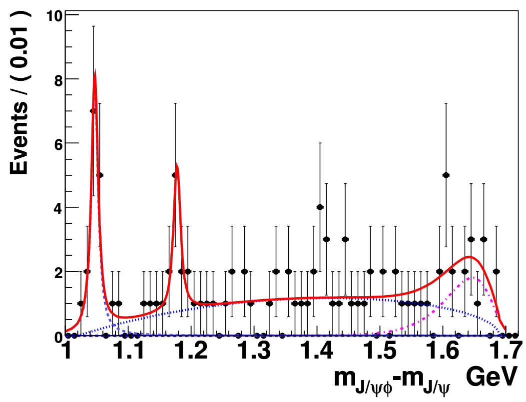

Figure 83: The null hypothesis fit to the mass difference between $J/\psi\phi$ and J/ψ in the defined B mass window assuming zero signal around the mass difference of 1.4 GeV.

5.9 Discussion of $J/\psi\phi$ Vs $J/\psi K^+K^-$

The relativistic BW shape for ϕ is shown in Fig. 84. The signal ratio between ϕ sideband ($|m_{K^+K^-} - m_\phi| > 0.007$ but in the range from 1.0 to 1.04 GeV/c^2) and our ϕ mass window ($|m_{K^+K^-} - m_\phi| < 0.007$) is 13.1%. The mass difference between $J/\psi\phi$ and J/ψ from ϕ sideband in the defined B mass window is shown in Fig. 85. We have 1 event around the $Y(4140)$. Assuming this is a real signal, the $Y(4140)$ signal yield ratio between ϕ sideband and our ϕ mass window is about $(1\pm1)/(15\pm4) = 7\%\pm7\%$, which is consistent with the ratio obtained from ϕ shape. That means that there is no evidence for $Y(4140) \to J/\psi K^+K^-$, however, this is statistic limited.

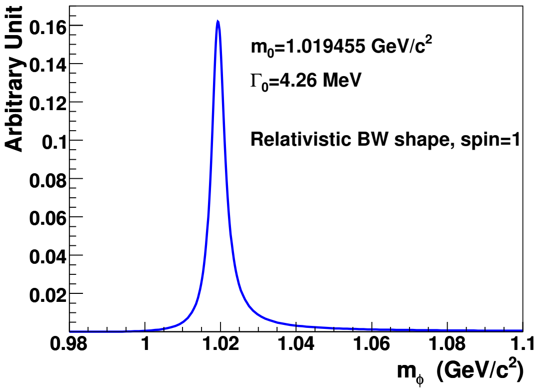

Figure 84: The relativistic BW shape for ϕ.

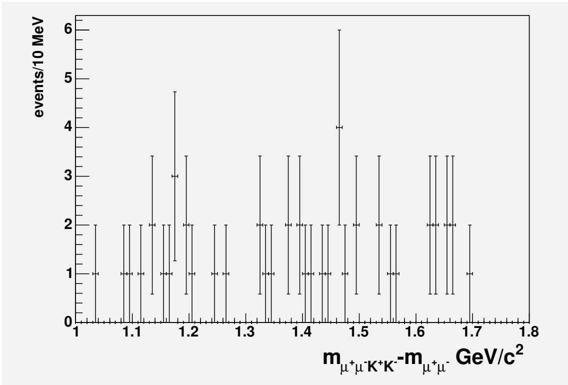

Figure 85: The mass difference between $J/\psi\phi$ and J/ψ from ϕ sideband in the defined B mass window.

5.10 Summary of Changes after Pre-bless

5.10.1 Require $p_T(K) > 400$ MeV/c and deal with track-splitting

Suggested by B group, we require $p_T(K) > 400$ MeV/c. The mass difference after this requirement is shown in Fig. 86. We found that there are two candidates from one event in Fig. 86 and this is due to track-splitting. These two candidates has same px/py/pz for the two muon tracks and the two tracks for ϕ candidate. The third kaon track has slightly different px/py/pz (0.0859689 -0.393141 0.0179407) GeV/c Vs (0.0856659 -0.391553 0.0179102) GeV/c. We only choose one candidate with higher vertex probability. The mass difference after this requirement will be shown in next section. The mass of $J/\psi\phi K^+$ after this requirement is shown in Fig. 87. A fit as before returns 75 ± 10 B^+ signal events.

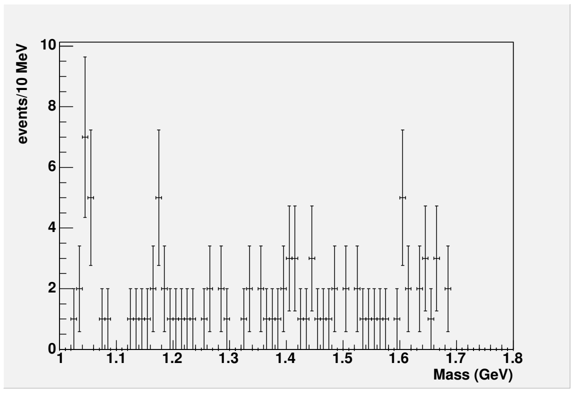

Figure 86: The mass difference between $J/\psi\phi$ and J/ψ in the defined B mass window after requiring $p_T(K) > 400$ MeV/c.

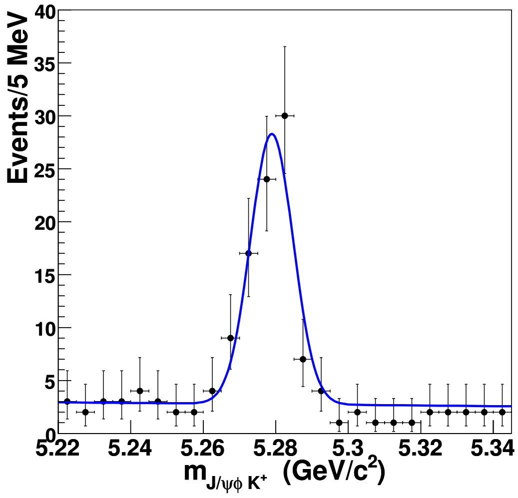

Figure 87: The mass of $J/\psi\phi K^+$ after requiring $p_T(K) > 400$ MeV/c.

5.10.2 Two new background shapes and Significance from Toy MCs

To avoid dealing with the $B_s \to \psi(2S)\phi$ contamination, we cut the mass difference spectrum up to 1.56 GeV/c^2. We choose the following signal and background PDF: S-wave relativistic BW [11] (ignoring resolution) for signal PDF and three-body-decay phase space as background shape. The signal and null hypothesis fits are shown in Figs. 88 and 89. The signal hypothesis fit returns mass difference, width and yield

[11] We use the form $\frac{m\Gamma(m)}{(m^2-m_0^2)^2+m_0^2\Gamma^2(m)}$, where $\Gamma(m) = \Gamma_0 \frac{q}{q_0}\frac{m_0}{m}$, and the 0 subscript indicates the value at the peak mass.

as 1046.4 ± 2.6 MeV/c^2, 11.9 ± 5.9 MeV and 14 ± 5. The log-likelihood difference between signal $2 \times \log(\mathrm{L_{max}})$ and null $2 \times \log(\mathrm{L_0})$ hypotheses is 28.0. The significance calculated by $\sqrt{2\ln(L_{max}/L_0)}$ is 5.3 sigma. The fit with a S-wave relativistic BW convoluted with a Gaussian resolution function with r.m.s fixed to 1.7 MeV obtained from MC signal PDF and three-body-decay phase space background PDF returns mass difference, width and yield as 1046.3 ± 2.9 MeV/c^2, 11.7 ± 5.7 MeV and 14 ± 5. and $2 \times \log(\mathrm{L_{max}})$ is 27.7. The effect caused by resolution is negligible. However, we use the values obtained from the fit with S-wave BW convoluted with a Gaussian resolution function as our central values after we collected comments from Collaboration.

Another background shape we investigated is flat combinatorial background shape plus three-body-decay phase space for non-resonant B decay background shape. By requiring the mass difference to be less than 1.56 GeV, we have 58 B signal events and 15 combinatorial background events in the defined B mass window as shown in Fig. 90. We normalize the flat background to 15 and then do a signal and null hypothesis fit to the mass difference spectrum. The signal hypothesis fit as shown in Fig. 91 returns mass difference, width and yield as 1046.6 ± 2.4 MeV/c^2, 10.8 ± 5.7 MeV and 13 ± 5. The log-likelihood difference between signal $2 \times \log(\mathrm{L_{max}})$ and null $2 \times \log(\mathrm{L_0})$ hypotheses is 23.2. The significance calculated by $\sqrt{2\ln(L_{max}/L_0)}$ is 4.8 sigma.

Since we do not have a precise theoretical prediction for this peak and its width, it can be anywhere in the mass difference spectrum and the width can be in a wide range. We use a MC simulation to include these factors and determine a p value. To save CPU time, we use the simple BW signal PDF in the fit for Toy MC. The corresponding $2ln(L_{max}/L_0)$ are 28.2 for three-body-decay phase space background shape and 23.6 for flat combinatorial background shape plus three-body-decay phase space background shape. For each MC trial for pure three-body-decay phase space background, we generate 73 events based on the background shape we used in the data, then do a signal and null hypothesis fit to the MC events to get the $-2\ln(\mathcal{L}_0/\mathcal{L}_{\mathrm{max}})$ value by floating the mass difference and width. In order to find the most significant fluctuation for one trial, we fit to the MC mass difference spectrum many times by setting a initial mass difference value every 50 MeV between 1.02 and 1.56 GeV for initial width of 50 MeV. We choose the maximum $-2\ln(\mathcal{L}_0/\mathcal{L}_{\mathrm{max}})$ to record from the above scan for each trial. We found 29 trials with $-2\ln(\mathcal{L}_0/\mathcal{L}_{\mathrm{max}})$ value equal or bigger than the value we obtained in the data. The p value determined by this MC simulation is 9.3×10^{-6}, which is about 4.3 σ significance. The p value obtained from 1.1 million MC simulation experiments for flat combinatorial background shape plus three-body-decay phase space background shape in the same way as pure three-body-decay phase space background shape is 9×10^{-5}, which is about 3.8 σ significance.

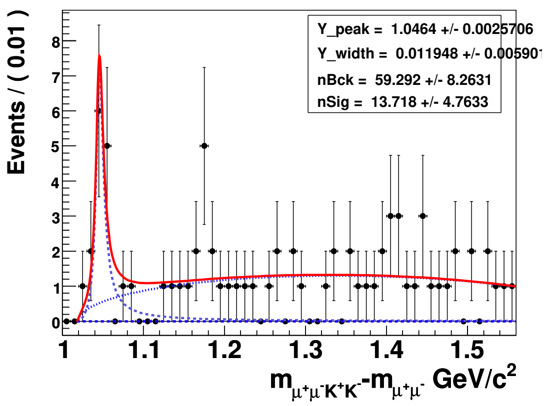

Figure 88: The signal hypothesis fit to mass difference between $J/\psi\phi$ and J/ψ in the defined B mass using relativistic S-wave BW signal PDF and three–body PS background PDF.

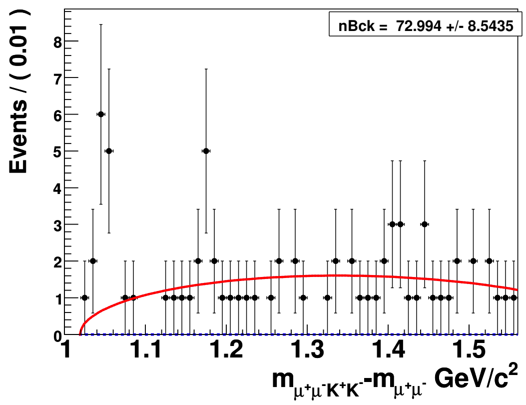

Figure 89: The null hypothesis fit to mass difference between $J/\psi\phi$ and J/ψ in the defined B mass using relativistic S-wave BW signal PDF and three–body PS background PDF.

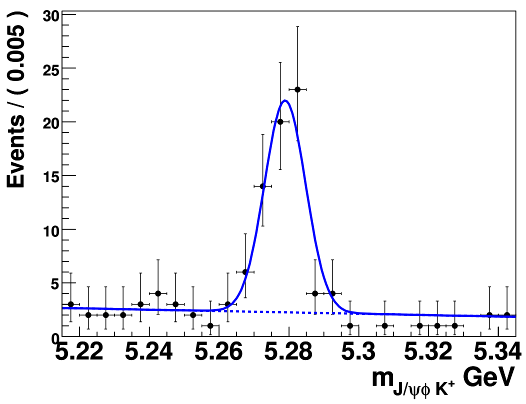

Figure 90: The $J/\psi\phi K^+$ mass spectrum after we require the mass difference to be less than 1.56 GeV/c^2.

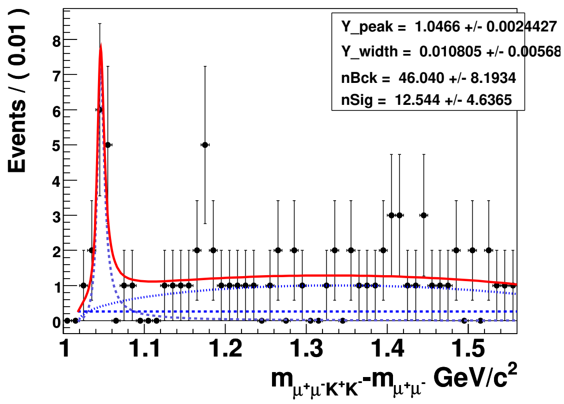

Figure 91: The signal hypothesis fit to mass difference between $J/\psi\phi$ and J/ψ in the defined B mass using relativistic S-wave BW signal PDF and three–body PS plus flat combinatorial background PDF.

5.10.3 Systematics

The returned mass differences and widths from the fit with different signal and background shapes are shown in Table 3. The biggest variations for mass difference and width from the central values are 1.2 MeV/$c^2$and 3.7 MeV, therefor we assign these values as systematics for mass difference and width.

Table 3: The returned parameters from the fit to the mass difference between $J/\psi\phi$ and J/ψ with different signal and background PDF assumptions.

signal PDF	background shape	Mass (MeV/c^2)	Width (MeV)
simple BW	3-body-PS	1047.4 ± 2.9	11.4 ± 5.3
simple BW	$q^3(Q^{1/2} + a_1 Q^{3/2})$	1047.5 ± 2.8	12.8 ± 5.3
simple BW	$q/(q + a_1 \times q)$	1047.4 ± 2.9	12.2 ± 5.4
S-wave relativistic BW	$q^3(Q^{1/2} + a_1 Q^{3/2})$	1046.2 ± 2.9	15.4 ± 7.5
S-wave relativistic BW	$q/(q + a_1 \times q)$	1046.2 ± 2.9	14.4 ± 7.7

5.10.4 Signal width and resolution convolution discussion

We perform fits to the mass difference distribution with an S-wave Relativistic BW described above and a Gaussian function with a width to be set to the resolution to test hypothesis that the structure at the $J/\psi\phi$ threshold to have zero width. The $-2\ln(\mathcal{L}_0/\mathcal{L}_{\max})$ value from these two fits is 11.4. Taking $-2\ln(\mathcal{L}_0/\mathcal{L}_{\max})$ as χ^2, the probability is 7×10^{-4}, or $\sqrt{(11.4)} = 3.4\,\sigma$ which means that the width of this structure is inconsistent with zero. We checked with an S-wave Relativistic BW convoluted with Gaussian function with rms fixed to 1.7 MeV and we got the same $-2\ln(\mathcal{L}_0/\mathcal{L}_{\max})$.

We ignored the resolution when we extract the structure's parameters using an S-wave Relativistic BW, as a cross check, we use an S-wave Relativistic BW convoluted with Gaussian function with rms fixed to 1.7 MeV and we obtained the following parameters: $\Delta M = 1046.3 \pm 2.9$ MeV/c^2, width=11.7 ± 5.7 MeV/c^2, yield=14 ± 5, and $-2\ln(\mathcal{L}_0/\mathcal{L}_{\max}) = 27.7$. Although the differences are negligible, we choose the values obtained from the fit with an S-wave Relativistic BW convoluted with Gaussian function with rms fixed to 1.7 MeV as our central values.

5.10.5 BF estimation

We observed 14 ± 5 $Y(4140)$ events from 75 B signal, so the ratio between $B^+ \to Y(4140)K^+, Y(4140) \to J/\psi\phi$ and $B^+ \to J/\psi\phi K^+$ is about 18.7% assuming the same efficiency between $B^+ \to J/\psi\phi K^+$ and $B^+ \to Y(4140)K^+$. We also generated the same amount of phase space $B^+ \to J/\psi\phi K^+$ MC and $B^+ \to Y(4140)K^+, Y(4140) \to J/\psi\phi$ (using the measured mass and width) to have a relative efficiency. However, we do not have official MC simulation for kaon PID, so we take off the pid cuts in the MC. The reconstructed MC events after the same requirements as in the data except the kaon PID are shown at Fig. 92 and 93. The relative reconstruction efficiency between $B^+ \to Y(4140)K^+, Y(4140) \to J/\psi\phi$ and $B^+ \to J/\psi\phi K^+$ is 344/311=1.106. Taking the BF of $B^+ \to J/\psi\phi K^+$ as 5.2×10^{-5} from PDG, the BF of $B^+ \to Y(4140)K^+, Y(4140) \to J/\psi\phi$ is estimated to be as $14/75/1.106 \times 5.2 \times 10^{-6} = 9.0 \times 10^{-6}$. Including the statistical uncertainty and PDG BF uncertainty, the BF of $B^+ \to Y(4140)K^+, Y(4140) \to J/\psi\phi$ can be expressed as: $(9.0 \pm 3.4(stat) \pm 2.9(BF)) \times 10^{-6}$. We kaon PID shows reasonable flat efficiency over kaon p_T (Fig. 94 and 95) by studying $B^+ \to J/\psi K^+$ control sample. Due to our large statistical uncertainty, we ignore systematics from PID and other possible sources.

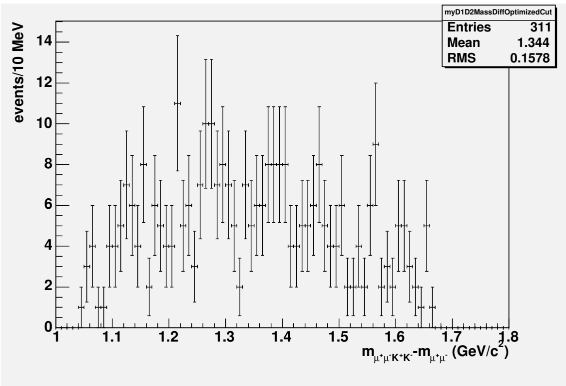

Figure 92: The reconstructed ΔM distribution from phase space $B^+ \to J/\psi\phi K^+$ MC as the same way as in the data but without kaon PID.

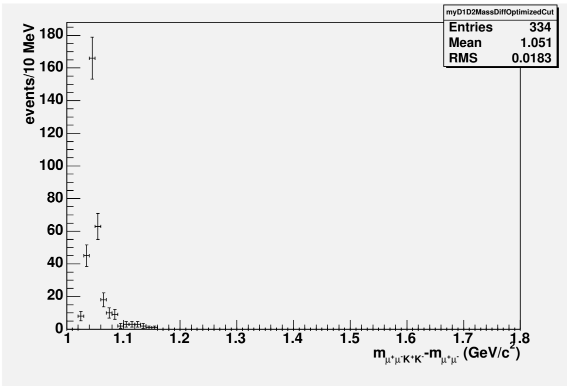

Figure 93: The reconstructed ΔM distribution from phase space $B^+ \to Y(4140)K^+, Y(4140) \to J/\psi\phi$ MC as the same way as in the data but without kaon PID.

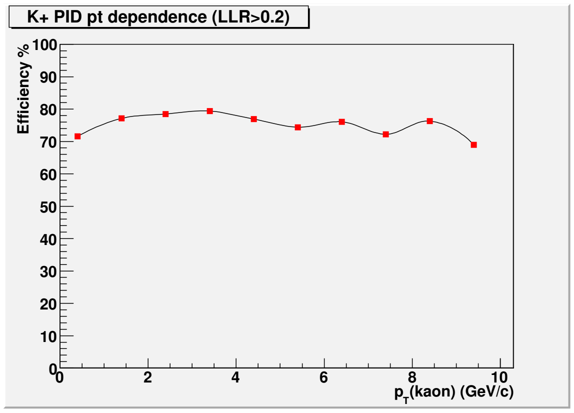

Figure 94: The K^+ PID efficiency as a function of kaon p_T using control sample $B^+ \to J/\psi K^+$ sample.

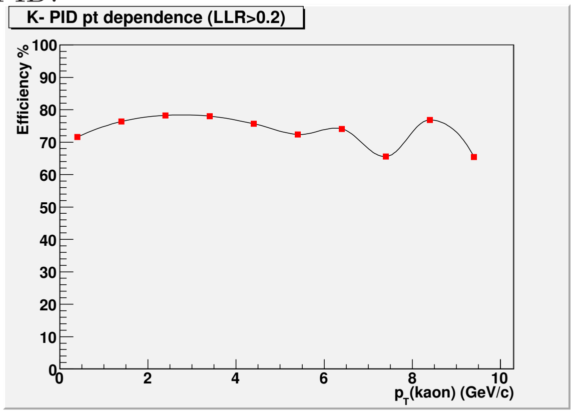

Figure 95: The K^- PID efficiency as a function of kaon p_T using control sample $B^+ \to J/\psi K^-$ sample.

5.10.6 The K^+K^- mass distribution inside B mass window

The $J/\psi\phi K^+$ mass before we require the mass window for J/ψ and ϕ is shown in Fig. 96. The sideband subtracted invariant mass of K^+K^- before J/ψ and ϕ mass requirements for $J/\psi\phi K^+$ inside 3 σ of the nominal B^+ mass is shown in Fig. 97. We use a P-Wave relativistic Breit-Wigner (BW) function [25] convoluted with a Gaussian resolution function with r.m.s fixed to 1.3 MeV obtained from MC (see below) only to do a χ^2 fit to the K^+K^- mass spectrum and it returns a mass of 1019.6 ± 0.3 MeV/c^2 and a width of 3.84 ± 0.65 MeV, which are consistent with ϕ's world average values [23]. This clean ϕ signal shows that the non-resonance K^+K^- component is negligible for $J/\psi\phi K^+$ signal. The MC K^+K^- mass distribution by setting ϕ's width to be zero is shown in Fig. 98, a Gaussian function only fit returns a resolution of 1.3 MeV.

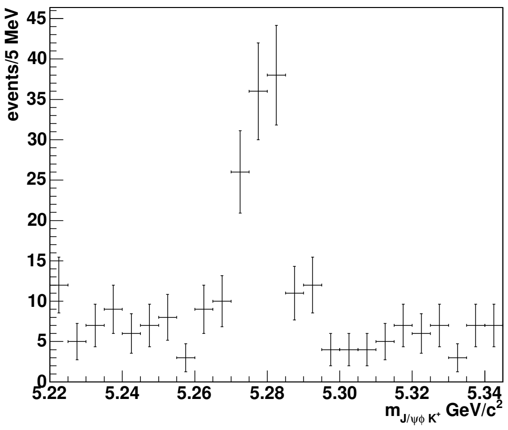

Figure 96: The $J/\psi\phi K^+$ mass before we require the mass window for J/ψ and ϕ but with all other requirements.

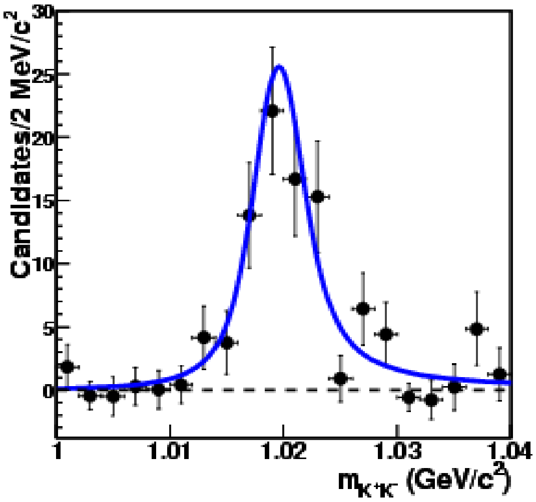

Figure 97: The sideband subtracted mass distributions of K^+K^- inside 3 σ of nominal B mass in $J/\psi\phi K^+$ mass distribution.

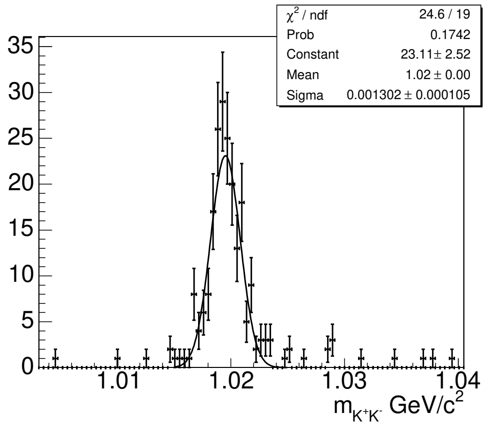

Figure 98: The MC mass distributions of K^+K^- by setting ϕ's width to be zero. A Gaussian function only fit returns a resolution of 1.3 MeV.

5.10.7 Cross check with relaxed cuts

As a cross check, we relax the following cuts as: $p(\chi^2)$ of B^+ vertex to be greater than 10^{-5}, the ϕ mass window as in range–[1.0,1.04] MeV, minimum kaon p_T as 250 MeV and minimum silicon hits as 3. The K^+K^- mass, $J/\psi\phi K^+$ and ΔM mass distributions are shown in Fig. 99. A fit to the ΔM distribution up to 1.25 GeV assuming two peaks (S-Wave relativistic BW) and three-body PS background as shown in Fig. 100 returns parameters as: $\Delta M1 = 1046.5 \pm 2.5$ MeV/c^2, width1=15.3 ± 6.0 MeV/c^2, yield1=27 ± 8; $\Delta M2 = 1178.6 \pm 3.1$ MeV/c^2, width2=18.7 ± 10.5 MeV/c^2, yield2=34 ± 13. More data is needed for a further study.

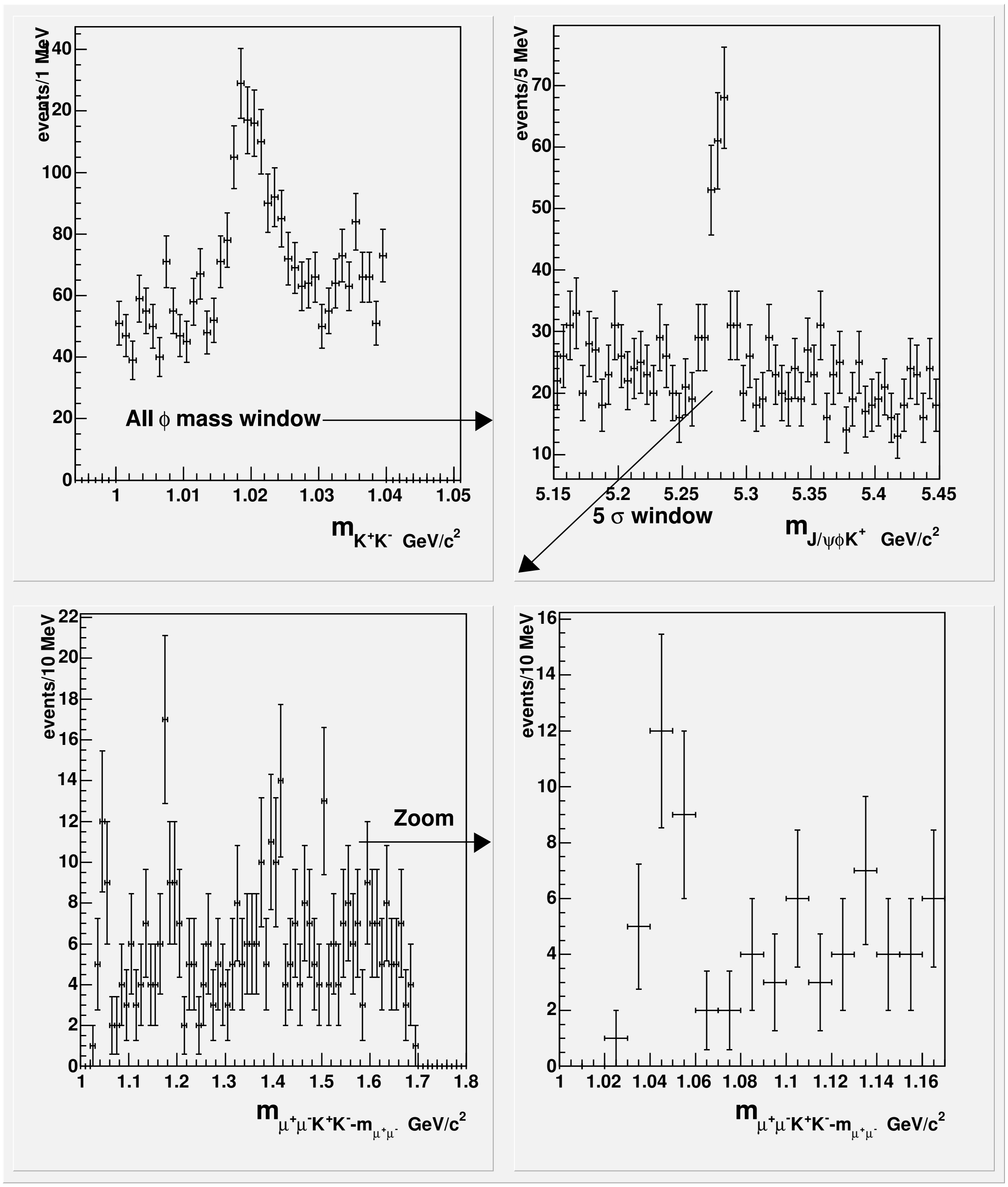

Figure 99: The K^+K^- mass, $J/\psi\phi K^+$ and ΔM mass distributions with relaxed cuts as a cross check.

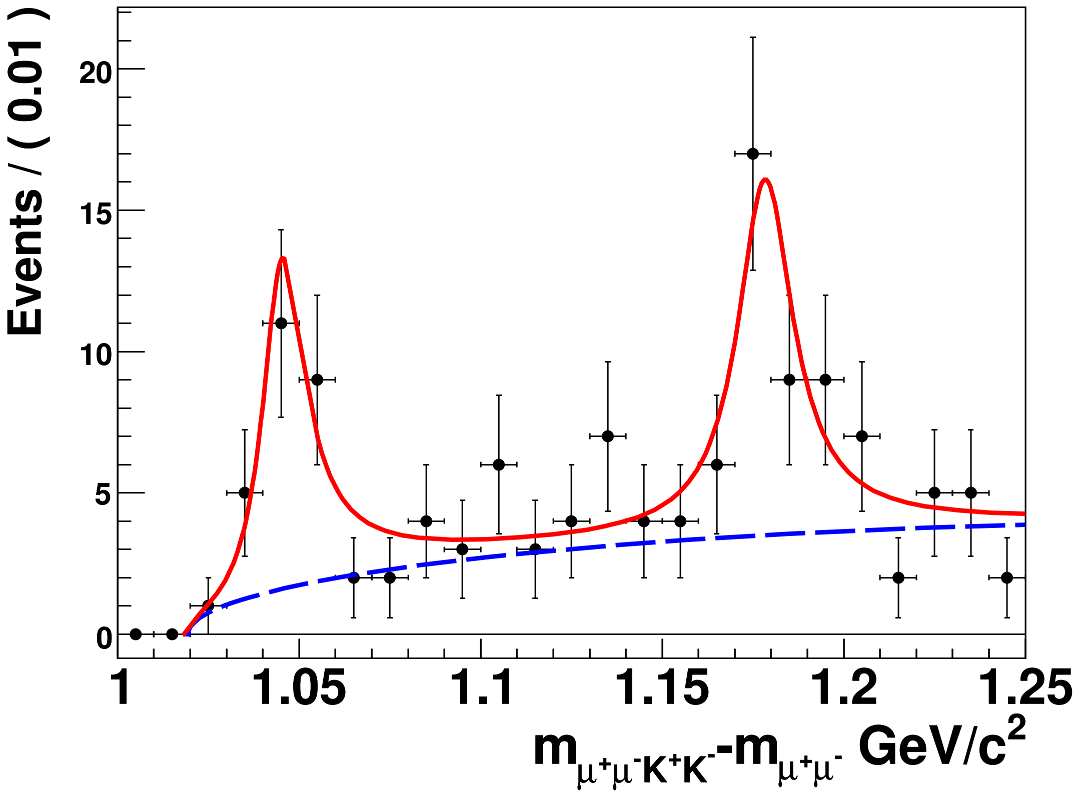

Figure 100: A fit to the ΔM distributions with relaxed cuts as a cross check (removed one candidate due to track-splitting).

5.10.8 Assigning asymmetric uncertainties to width

Suggested by Karlsruhe group, we did a LLR scan with the width of the structre and assign asymmetric uncertainties to the width. The scan is listed in Table 4. We assign the uncertainties as $^{+8.3}_{-5.0}$ MeV determined by changing $2\Delta lnL$ by 1 unit.

Table 4: The $2\Delta lnL$ distribution comparing with 11.7 MeV case as a function of width.

Width value (MeV)	$2\Delta lnL$ comparing with 11.7 MeV
23	1.5
20	1.0
16.5	0.4
14.7	0.2
11.7	0.0
9.0	0.3
6.7	1.0
6.0	1.4
3.0	4.7
1.0	9.1
0.0	11.4

5.11 Discussion of X(4160)

Recently Belle reported a structure called X(4160) with positive C parity [3], the mass of X(4160) is close to the structure in the $J/\psi\phi$ threshold but its width is much wider with large uncertainty. The PDFs of the two structures are shown in Fig. 101. Considered the narrowness of the structure in the $J/\psi\phi$ threshold, they are not likely to be the same.

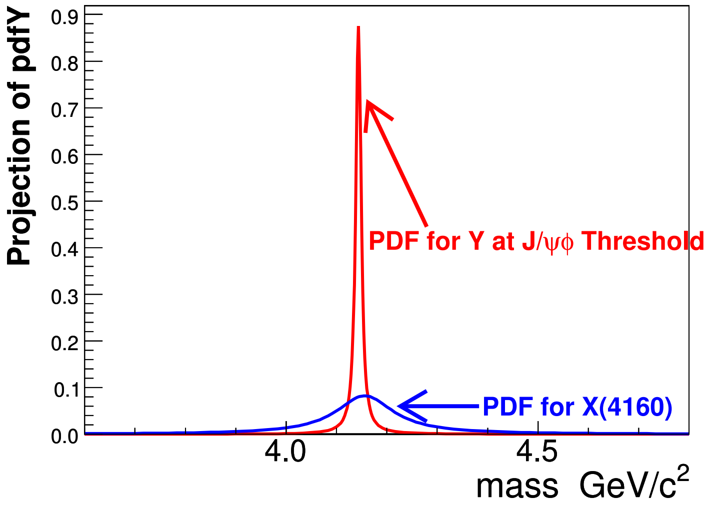

Figure 101: The PDF comparison between X(4160) and the structure in $J/\psi\phi$ threshold.

6 Summary and Acknowledgment

We see evidence for a structure decays into $J/\psi\phi$ at its threshold from exclusive $B^+ \to J/\psi\phi K^+$ decays. The mass of this structure is measured as $4143.0 \pm 2.9(\text{stat}) \pm 1.2(\text{syst})$ MeV/c^2 and its width is measured as $11.7^{+8.3}_{-5.0}(\text{stat}) \pm 3.7(\text{syst})$ MeV/c^2, the C parity of this structure is positive. Since its mass is above the open charm pair threshold, normal charmonium is not preferred to decay into this channel, the explanation of this structure is open to more interesting possibilities.

We would like to thank many CDF colleges for their generous help: Gerry, Christoph, Elisa, Jennifer, Pat, Michal, Giovanni, Manfred, Jacob, Doug, Rob, Ted, Tom, PID people and many more!

References

[1] S. K. Choi *et al.* (Belle Collaboration), *Phys. Rev. Lett.* **91** (,) 262001 (2003); D. Acosta *et al.* (CDF Collaboration), *Phys. Rev. Lett.* **93** (,) 072001 (2004); V. M. Abazov *et al.* (D0 Collaboration), *Phys. Rev. Lett.* **93** (,) 162002 (2004); D. Aubert *et al.* (BaBar Collaboration), Phys. Rev. D **71**, 071103(R) (2005). 4

[2] S.-K. Choi *et al.* (Belle Collaboration), *Phys. Rev. Lett.* **94** (,) 182002 (2005); D. Aubert *et al.* (BaBar Collaboration), 0711.2047[hep-ex]. 4

[3] P. Pakhlov *et al.* (Belle Collaboration), *Phys. Rev. Lett.* **100** (,) 202001 (2008). 4, 54

[4] D. Aubert *et al.* (BaBar Collaboration), *Phys. Rev. Lett.* **95** (,) 142001 (2005). 4

[5] D. Aubert *et al.* (BaBar Collaboration), *Phys. Rev. Lett.* **98** (,) 212001 (2007). 4

[6] X. L. Wang *et al.* (Belle Collaboration), *Phys. Rev. Lett.* **99** (,) 142002 (2007). 4

[7] S. K. Choi *et al.* (Belle Collaboration),*Phys. Rev. Lett.* **100** (,) 142001 (2008), R. Mizuk, R. Chistov *et al* (Belle Collaboration), 0806.4098[hep-ex]. 4

[8] K. F. Chen *et al.* (Belle Collaboration),*Phys. Rev. Lett.* **100** (,) 112001 (2008). 4

[9] E. Eichten, K. Lane, C. Quigg, Phys. Rev. D **69**, 094019, (2004). 4

[10] S. L. Zhu, Phys. Lett. B **625**, 212 (2005); F. Close, P. Page, Phys. Lett. B **628**, 215 (2005); 4

[11] E. Swanson, Phys. Lett. B **588**, 189, (2004); 4

[12] L. Maiani, F. Piccinini, A. D. Polosa, and V. Riquer, Phys. Rev. D **72** (R), 031502(R) (2005). 4

[13] E. J. Eichten, Charm workshop 2007. 4

[14] P. Hasenfratz, R. R. Horgan, J. Kuti, and J. -M. Richard, Phys. Lett. B **95**, 299 (1980); S. Perantonis and C. Michael, Nucl. Phys. B **347**, 864, (1990); 4

[15] C. Bernard *et al.*, Phys. Rev. D **56**, 7039, (1997); X. Liao and T. Manke, hep-lat/0210030. 4

[16] A. Anastassov *et al.* (CLEO Collaboration), *Phys. Rev. Lett.* **84** (,) 1393 (2000); 4

[17] B. Aubert *et al.* (BaBar Collaboration), *Phys. Rev. Lett.* **91** (,) 071801 (2003). 4

[18] F. E. Close *et al.*, Phys. Rev. D **57**, 5653, (1998);
F. E. Close *et al.*, hep-ph/0305285. 4

[19] S. J. Brodsky, I. Schmidt, and G. Teramond, *Phys. Rev. Lett.* **64** (,) 1011 (1990). 4

[20] C. R. Nappi, Phys. Rev. D **25**, 25, (1982); E. L.Berger, G. T. Bodwin, and J. Lee, hep-pj/0206115; E. L.Berger, hep-ph/0209374. 4

[21] S. Chang, P. J. Fox, N. Weiner, hep-ph/0608310v1. 4

[22] Kai Yi *et al.*, CDF note 6160. See Fig. 19. 4

[23] C. Amsler *et al.* (Particle Data Group), Phys. Lett. B **667**, 1 (2008). 48

[24] M. Pivk and F. R. Le Diberder, Nucl. Instrum. Meth. A **555**, 356 (2005). 32

[25] B. Aubert *et al.* (BaBar Collaboration), Phys. Rev. D **78**, 071103 (2008). 48